Mineralogy and chemistry of altered Icelandic basalts: Application to clay mineral detection and understanding aqueous environments on Mars

B. L. Ehlmann,[1,2] D. L. Bish,[3] S. W. Ruff,[4] and J. F. Mustard[5]

Received 6 June 2012; revised 16 August 2012; accepted 20 August 2012; published 13 October 2012.

[1] We used a suite of techniques, including those emulating compositional data sets obtained from Mars orbit and obtainable at the Mars surface, to examine aqueous alteration of basaltic rocks from Iceland as a mineralogic and geochemical analog for Noachian environments on Mars. A sample suite was collected for laboratory measurement of (1) whole-rock visible/near-infrared (VNIR) reflectance and thermal infrared (TIR) emission spectra; (2) VNIR and TIR reflectance spectra of particle-size separates derived from the bulk rock and from materials extracted from fractures/vesicles; (3) X-ray diffraction (XRD) patterns for determination of quantitative modal mineralogy; (4) major element chemistry using flux fusion of whole-rock powders; and (5) electron microprobe analyses of minerals in thin sections. Conclusions about aqueous alteration can be influenced by technique. For these basalts, whole-rock chemical data showed scant evidence for chemical fractionation, but TIR, VNIR, and XRD measurements identified distinctive assemblages of hydrous silicate minerals, differing by sample. XRD provided the most complete and accurate quantitative determination of sample mineralogy. However, VNIR spectroscopy was the technique most useful for determining composition of low-abundance smectite clays, and TIR spectroscopy was the most useful for recognizing hydrated silicates in thin surface coatings. High spatial resolution mineralogical and chemical data sets were useful for understanding the texture and distribution of alteration products and variations in fluid chemistry. No single approach provides a complete assessment of the environment of alteration, demonstrating the importance of employing multiple, synergistic mineralogical and geochemical techniques and instruments in exploration of rock strata from aqueous paleoenvironments on Mars.

Citation: Ehlmann, B. L., D. L. Bish, S. W. Ruff, and J. F. Mustard (2012), Mineralogy and chemistry of altered Icelandic basalts: Application to clay mineral detection and understanding aqueous environments on Mars, *J. Geophys. Res.*, *117*, E00J16, doi:10.1029/2012JE004156.

1. Introduction

[2] Investigations of paleoenvironment in terrestrial geology benefit from the ability to employ multiple measurement techniques, including quantification of rock modal mineralogy, examination of small-scale petrographic textures down to nanometer-scale, and high-precision and spatial resolution geochemical and isotopic analyses. In contrast, geologic investigations of Mars' past aqueous environments occur in a comparatively data-poor environment. Bulk chemical data have been acquired at six landing sites, sometimes accompanied by thermal emission and Mössbauer spectroscopy or thermal gravimetric data for mineralogic information. Planet-wide, thousands of discrete exposures of rocks with secondary minerals have been detected from orbit with thermal emission and visible/near-infrared reflectance spectroscopy [*Christensen et al.*, 2001; *Bibring et al.*, 2006; *Murchie et al.*, 2009]. Consequently, much interpretation of Mars' paleoenvironmental conditions relies on these remote sensing data sets.

[3] Expertise in the interpretation of remote sensing data sets can be acquired via examination and subsequent verification of spectroscopic data sets from terrestrial analog sites. Most recent investigations of Mars-analogue sites have focused on sulfur-rich, acidic systems likely typical of Hesperian (3.1–3.7 Gyr) Martian environments, e.g., the Hawaiian volcanoes, Australian acid lakes, and Rio Tinto, Spain [e.g., *Morris et al.*, 2005;

[1]Geological and Planetary Sciences, California Institute of Technology, Pasadena, California, USA.
[2]Jet Propulsion Laboratory, California Institute of Technology, Pasadena, California, USA.
[3]Department of Geological Sciences, Indiana University, Bloomington, Indiana, USA.
[4]School of Earth and Space Exploration, Arizona State University, Tempe, Arizona, USA.
[5]Department of Geological Sciences, Brown University, Providence, Rhode Island, USA.

Corresponding author: B. L. Ehlmann, Geological and Planetary Sciences, California Institute of Technology, Pasadena, CA 91125, USA. (ehlmann@caltech.edu)

0148-0227/12/2012JE004156

Fernández-Remolar et al., 2005; *Schiffman et al.*, 2006; *Benison et al.*, 2007; *Hurowitz and McLennan*, 2007; *Seelos et al.*, 2010; *Hamilton et al.*, 2008]. We have undertaken a study of the alteration of basalt lava flows in Iceland as a potential mineralogic and geochemical analogue for neutral to alkaline pH alteration of the basaltic terrains of Noachian Mars.

[4] Hydrated silicate minerals, specifically Fe/Mg smectite clays, are commonly recognized in Noachian (>3.7 Gyr) terrains on Mars and are globally widespread [*Poulet et al.*, 2005; *Mustard et al.*, 2008; *Ehlmann et al.*, 2011a]. They were first detected using the Observatoire pour la Minéralogie l'Eau les Glaces et l'Activité (OMEGA), an orbiting visible/near-infrared (VNIR) imaging spectrometer (0.4–5 μm, 300–1000 m/pixel) [e.g., *Bibring et al.*, 2005] on the Mars Express spacecraft. Subsequent data at 18 m/pixel scale, obtained from the Compact Reconnaissance Imaging Spectrometer for Mars (CRISM; 0.4–4 μm, 18–200 m/pixel) [*Murchie et al.*, 2007] on the Mars Reconnaissance Orbiter spacecraft revealed distinctive assemblages of hydrated silicate minerals that indicate past aqueous alteration in diverse environments, including at neutral to alkaline pH [*Poulet et al.*, 2005; *Mustard et al.*, 2008; *Murchie et al.*, 2009; *Ehlmann et al.*, 2011a]. Clay minerals require long-term interaction of water and rock to form, pointing to persistent environments with liquid water. Assemblages, including Fe/Mg smectites, chlorite, opaline silica, and zeolites, have been detected in Noachian cratered terrains and have been inferred to represent evidence for low water:rock ratio alteration in subsurface hydrothermal systems [*Ehlmann et al.*, 2009; *Carter et al.*, 2010; *Ehlmann et al.*, 2011a, 2011b]. Elsewhere, rocks containing aluminum-rich clays have been found stratigraphically above iron-magnesium clay-bearing rocks and may represent pedogenic (top-down leaching) environments on early Mars [*Wray et al.*, 2008; *Bishop et al.*, 2008a; *Ehlmann et al.*, 2009; *Murchie et al.*, 2009; *Loizeau et al.*, 2010; *Michalski et al.*, 2010a; *Ehlmann et al.*, 2011a]. Initial VNIR studies of the abundance of clay minerals in the largest discovered exposures gave estimates of 15–65% [*Poulet et al.*, 2008].

[5] In many of these regions of clay mineral detections, thermal infrared (TIR) spectra (~6–50 μm; ~1600–200 cm^{-1}) from the orbiting Thermal Emission Spectrometer (TES) [*Christensen et al.*, 2001] on the Mars Global Surveyor spacecraft show no unambiguous evidence for such phases, perhaps due in part to the larger spatial footprint of 3 km × 5 km. Some Noachian terrains show emissivity minima at longer wavelengths (16–25 μm, 600–400 cm^{-1}) that are characteristic of high silica materials [*Ruff and Christensen*, 2007] and/or poorly crystalline amorphous materials with minor <15% phyllosilicate content [*McDowell and Hamilton*, 2009; *Michalski and Fergason*, 2009]. Clay mineral abundances of 10–30% in Noachian terrains have been noted for one location [*Michalski et al.*, 2010b], but the detection of clay minerals using the TES data set is uncommon. A third remote sensing data set, chemical measurements provided by the Gamma Ray Spectrometer (GRS), shows little evidence for chemical fractionation, e.g., depletion and concentration of elements caused by aqueous alteration, at 5° × 5° spatial scale [*Taylor et al.*, 2010].

[6] The relative prevalence of clay mineral detections in VNIR global data sets versus the paucity of definitive identifications in TIR global data sets and lack of chemical evidence for widespread weathering is puzzling. Each data set, considered alone, might lead to a different conclusion about the style, prevalence, and longevity of aqueous alteration on Mars. In reality, each data set is influenced differently by the quantity, texture, and exposure of mineral phases and, consequently, provides different constraints on the composition of clay-bearing terrains. Understanding how to utilize these and other data sets in tandem and limitations to what is knowable or unknowable from each is important, especially given that remote sensing data are utilized to interpret Martian paleoenvironmental conditions, select landing sites, and guide rover exploration. Indeed, the 2011 Mars Science Laboratory (MSL) rover is scheduled to land in Gale crater, selected in part because of the detection of clay-bearing sediments in VNIR orbital data [*Milliken et al.*, 2010]. At Gale Crater, the MSL rover will deploy a suite of instruments to assess mineralogy and elemental chemistry, including CheMin, an X-ray diffraction/X-ray fluorescence (XRD/XRF) spectrometer, ChemCam, a remote sensing laser-induced breakdown spectrometer for elemental chemistry, and an alpha proton X-ray spectrometer (APXS) for elemental composition [*Grotzinger et al.*, 2012]. In this context, we examine how conclusions about alteration environment drawn from orbital infrared spectral data (VNIR and TIR) compare with information obtained via in situ techniques like those of MSL. We supplement these with techniques that could be used on future landed missions and one that is presently restricted to terrestrial laboratories (electron microprobe).

[7] We examined rocks collected from Icelandic basalt flows that were in some places altered at the surface by pedogenesis and in other locations were hydrothermally altered by non-marine, non-sulfurous groundwater circulation. Our sample characterization methods compared mineralogy determined with infrared spectroscopy of whole rocks (comparable to Mars orbital data from CRISM, OMEGA, and TES and rover data from the Miniature Thermal Emission Spectrometer (MiniTES)) [*Christensen et al.*, 2003] with information derived from in situ data: small-scale infrared spectroscopy, elemental chemistry, and mineralogy from X-ray diffraction. Key questions driving this study were to what extent do remote spectroscopic approaches permit a complete understanding of weathering and alteration? What are the advantages and limitations of particular remote and in situ techniques for determination of clay mineralogy? Do additional in situ data change spectroscopic mineral identifications and/or paleoenvironmental interpretations? What are the synergies among different techniques and data sets for remote compositional analysis? After reviewing the geologic setting of the chosen Iceland analog site and detailing methodology, we describe results from each technique and implications for use of orbiter and rover data in interpreting the mineralogy and paleoenvironments of Mars.

2. Geologic Setting

[8] The land surface of Iceland consists of poorly formed soils, bare rock, and sparse vegetation. Extrusive basaltic lava flows, emplaced over the last 16 Myr, comprise 85% of the bedrock [*Gislason et al.*, 1996]. Most Icelandic hydrologic systems are fed by waters that originate from precipitation, rather than being derived from seawater. A variety of geothermal spring systems (low

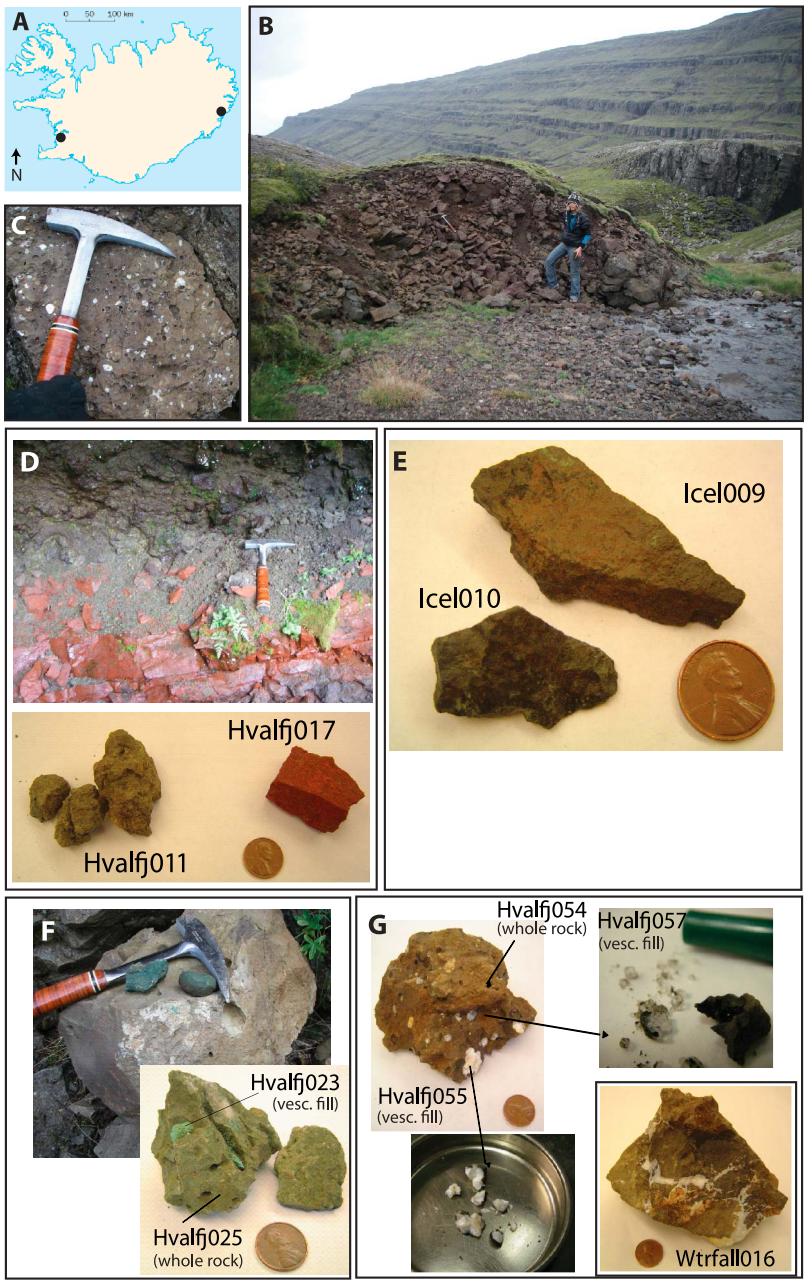

Figure 1. Sampling sites and study samples. (a) Rocks were sampled near Hvalfjordur (west) and Berufjordur (east). At both sites, massive basaltic flows exhibited evidence of alteration minerals filling veins and fractures. (b) Successive basalt flows eroded by glacial activity and a stream at Berufjordur, site of sample wtrfall016. (c) Outcropping of zeolitized basalt at Hvalfjordur. (d) Hvalfj011 and hvalfj017 sample friable materials cut by a stream within a gray unit and red unit and may represent a contact between two lava flows, the lower with paleosol development. (e) Icel009 and icel010 sample massive basalt outcrops in western Iceland. (f) Hvalfj023 and hvalfj025 sample a basaltic rock with blue-green vesicle fill. (g) Hvajfl054, havlfj055, and hvalfj057 sample two types of filled vesicles and the bulk rock of a typical brownish, zeolitized basalt. (inset) Wtrfall016 samples white mineral filling fractures in altered basalt from Berufjordur.

temperature, low sulfur; low temperature, high sulfur; and high temperature, high sulfur) with distinctive pH, Eh, and aqueous geochemistries create diverse assemblages of secondary minerals [e.g., *Kristmannsdottir*, 1976; *Gislason and Eugster*, 1987; *Lonker et al.*, 1993; *Arnórsson*, 1995a, 1995b; *Gislason et al.*, 1996; *Franzson et al.*, 2008].

[9] Rocks from two localities were studied here (Figure 1). The Hvalfjordur basalt succession (64.3°N, 21.7°W) consists of 3–4 Myr plateau basalts that have been subjected to zeolitic-grade alteration [*Neuhoff et al.*, 1999; *Franzson et al.*, 2008; *Weisenberger and Selbekk*, 2009]. The Berufjordur plateau sequence (64.8°N, 14.5°W) is older, ~9–11 Myr,

based on dating of nearby sequence members [*Kissel et al.*, 2010], and exhibits similar hydrothermal alteration. The two study areas differ from younger (<3.3 Myr) volcanic successions because they lack hyaloclastite formations, which are characterized by the presence of palagonite, formed during volcano-ice interactions and have been previously examined as Mars analogues [*Bishop et al.*, 2002a]. The samples in this study are volcanic rocks buried by accumulation of younger volcanics. The environments of aqueous alteration for these rocks include weathering at relatively low temperatures at or near the surface; hydrothermal alteration in heated environments near the surface, driven by emplacement of hot overlying lavas from subsequent eruptions; and/or alteration of minerals by burial and heating by the geothermal gradient. Both study sites are not near central volcanoes or volcanic vents and lacked sulfide or sulfate mineral phases, and thus altering fluids were not sulfurous. Tens to hundreds of meters of glacial and fluvial erosion have exposed deep parts of the basalt sequence.

3. Methods

[10] The approach during fieldwork was to select samples of different color, coherency, fracture-fill style, and VNIR spectral characteristics (described below) with emphasis on capturing the diversity at the site. From the collected samples, representative basalts with both massive and vesicular textures and different styles of alteration were then selected for further detailed study (Figure 1). Hvalfj011 and hvalfj017 were sampled from the boundary between two lava flows and are fairly homogenous at hand sample scale, but they are weak, friable, and visibly altered. Hvalfj023, hvalfj054, and wtrfall016 are heterogeneous and were selected as end-members of basalt clearly altered by precipitation of minerals in veins and vesicles. Icel009 and icel010 are homogenous at hand sample scale, have a somewhat waxy feel, and are typical of hard, coherent basalt (no fracture fill).

[11] Initial whole-rock spectra acquired with an Analytical Spectral Devices (ASD) field spectrometer (described in section 3.4) show evidence for hydrous phases, indicated by absorptions at 1.4 and 1.9 μm (Figure 2a). There is also variation in the character of Fe-related electronic transition absorptions at wavelengths <1.5 μm. OH and metal-OH overtones and combination bands of varying strength are also visible near 1.4 μm and in the 2.0–2.6 μm region. Absorption feature positions and strengths for the sample suite are broadly similar to those in spectra from which mineral identifications have been made on Mars, including "Fe, Mg phyllosilicate," "montmorillonite," "silica," "zeolite," and, "hydrated" types (Figure 2b). Continuum shape is markedly different because of the lower H_2O content of materials on the Mars surface versus Earth's surface, i.e., the downward slope in long-wavelength data toward the 3-μm H_2O fundamental stretch is less pronounced for Mars data and the continuum shortward of ~1.5 um is also influenced by dehydration [see also *Morris et al.*, 2011].

[12] Measurements were performed in the laboratory to determine sample mineralogy and chemistry, to understand the record of alteration processes, and to understand how alteration environment is revealed (or not) using different mineralogical and chemical measurement techniques. VNIR and TIR spectral analyses were conducted on whole rocks and particle size separates to simulate remote sensing measurements acquired at orbital to outcrop to microscopic spatial scales. XRD and flux fusion elemental analyses were employed, providing data similar to those measurable in situ on Mars, and electron microprobe measurements were acquired to obtain the highest fidelity understanding of mineral composition. IR spectral analyses were performed without utilizing a priori knowledge of mineral composition from XRD and microprobe data. Below, we detail methods for each analysis technique.

3.1. XRD

[13] Samples of the bulk rock and fracture/vesicle fill were extracted from each rock (Figure 1) and were then ground with a mortar and pestle. X-ray diffraction (XRD) measurements were made on <25 μm size fraction samples over a 2θ range of 2° to 70° at 0.02° 2θ intervals using a Bruker D8 Advance diffractometer at Indiana University with Cu Kα radiation, incident- and diffracted-beam Soller slits, and a solid-state PSi detector. All samples were initially measured with count times of 2s per 0.02°2θ step, and selected samples were re-measured with 15 s count times to improve counting statistics. Data for untreated samples simulate those that will be acquired on Mars by the CheMin XRD/XRF instrument on MSL, although the CheMin instrument will use Co radiation instead of Cu and has a useful 2θ range of 5° to 55° [*Blake et al.*, 2010].

[14] Areas of the most intense peaks from component minerals were measured, and the relative percentage of each constituent was determined using the reference intensity ratio (RIR) method [*Chung*, 1974], using literature RIR values and values measured in laboratory. Rietveld refinement was also applied, using the Topas Rietveld program, to determine the relative abundance of the well-ordered (i.e., non-clay minerals) components. The Rietveld modeling method allows refinement of unit-cell parameters for component minerals, and it also provides information on crystallite size and strain contributions to peak broadening [*Bish and Post*, 1993]. Contributions from smectite were not calculated using the Rietveld method because the mineral is not three-dimensionally ordered and is not properly modeled by the Topas program. Final calculated abundances represent weight percents obtained from the Rietveld method scaled to include the RIR-determined abundances of phases without three-dimensional ordering, e.g., smectites. Past studies indicate that errors associated with mineralogic quantification are approximately ±10% relative; the detection limit for well-ordered phases is generally <2% but depends on count time and the phase [*Bish and Chipera*, 1991].

[15] Additional measurements and sample preparations were done to determine as precisely as possible the composition of clay minerals in the samples. All samples containing clay minerals were measured with 15s count times over the 2θ range of 58° to 64° to measure the 060 reflection. The positions and magnitudes of reflections in this region are typically used to facilitate discrimination between dioctahedral and trioctahedral smectites based on the size of their *b* unit-cell axes [*Moore and Reynolds*, 1997]. To verify the presence of smectite clays and check for possible interstratified or non-expanding clays in five of the ground bulk-rock samples that possessed low-angle diffraction peaks, <2 μm size separates were produced by timed settling in

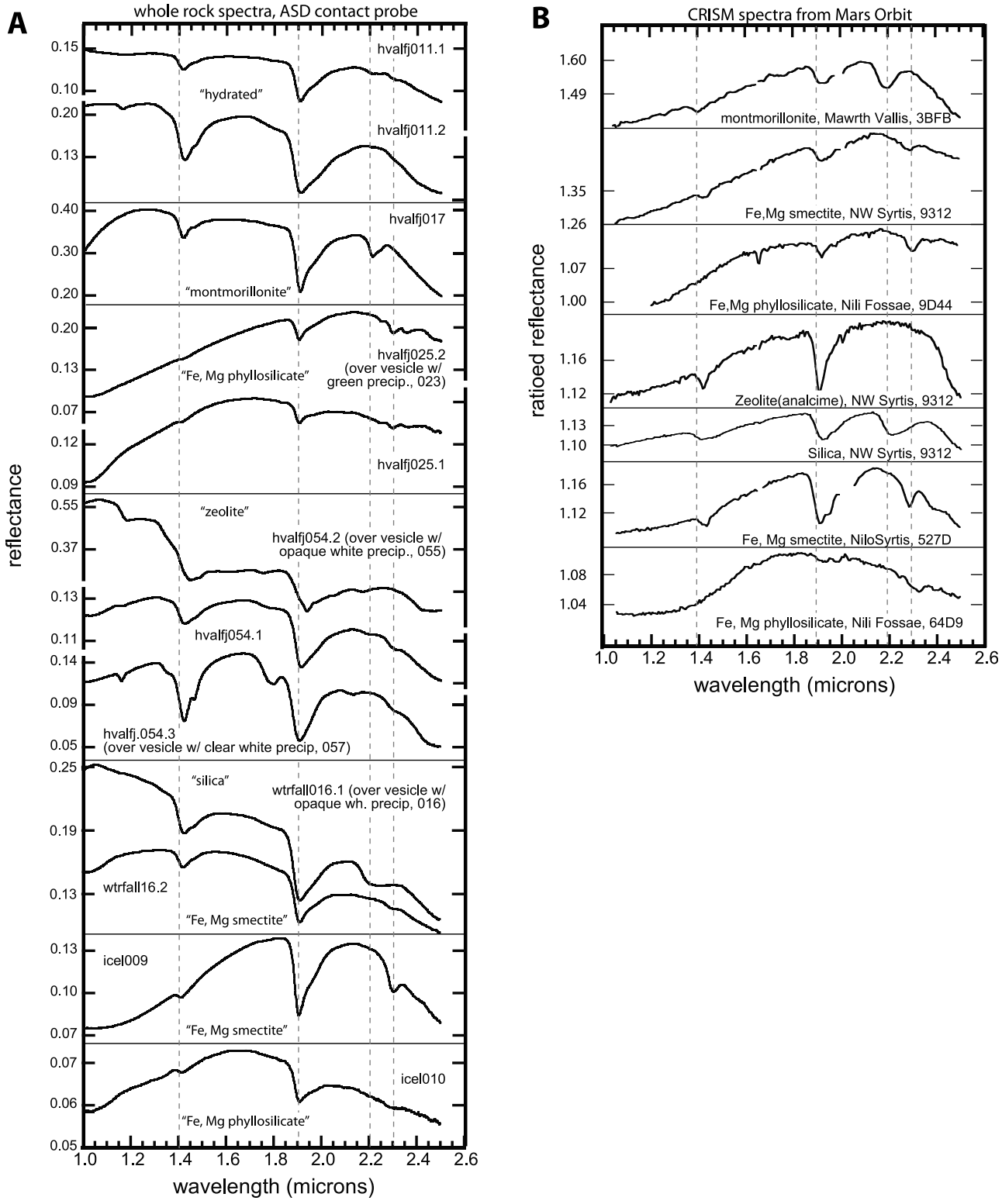

Figure 2. Spectra from Iceland and Mars. (a) ASD spectra of whole rocks displayed in Figure 2 from 1.0 to 2.6 μm. Spectra from multiple rock faces were acquired with a contact probe attachment ($\sim$2 cm diameter field of view), and multiple spectra are shown where there were substantial spectral differences between parts of the rock. (b) Select spectra from basaltic terrains on Mars, exhibiting evidence for aqueous alteration and spectra similar to those from Icelandic rocks. Ratioed spectra are shown from *Mustard et al.* [2008] and *Ehlmann et al.* [2009]with the inferred mineral, location on Mars, and image ID (leading four zeros omitted).

water [*Chipera et al.*, 1993]. These separates were not washed with different solutions, nor heated. These untreated <2 μm samples were prepared as oriented mounts on off-axis cut quartz plates, dried, saturated with ethylene glycol, and then measured from 2 to 20° 2θ. Incorporation of ethylene glycol molecules into the interlayer of smectites causes the 001 spacing to expand to ~16.7Å, whereas non-expanding clays such as chlorite, illite, and kaolinite do not experience a peak shift. Patterns from oriented, glycolated samples were examined for irrationality of higher-order reflections that would indicate the presence of interstratification. These procedures are not currently possible to do remotely (e.g., on MSL on Mars) but are a best-practices laboratory means to obtain the precise composition of smectites in our samples, thus providing a check of our infrared spectroscopic and bulk-rock XRD mineralogic data.

3.2. Elemental Analysis

[16] Flux fusion of powdered samples followed by inductively coupled atomic optical emission spectrometry (ICP-AOES) measurements at Brown University were used to measure the weight percent of Al, Ca, Fe, K, Mg, Mn, Na, Si, and Ti using the procedures outlined in *Murray et al.* [2000]. For each sample (<150 μm size fraction), 40 mg of ground and dried sample was mixed with lithium metaborate flux in a 4:1 flux-to-sample ratio in a graphite crucible. The mixture was then fused in a furnace at 1050°C for 10 min. The fused bead was poured into a bottle with 10% nitric acid and agitated for >30 min to promote dissolution. The sample solution was then filtered through a 0.45 μm filter to remove graphite and diluted to 4000× for analysis by ICP-AOES. Unknown samples were run in triplicate along with three blanks and eight standard reference samples. ICP data were corrected for drift over the measurement run and for matrix effects using the blanks, and results were converted to elemental weight percent. These data were then multiplied by a correction factor to account for losses due to the flux fusion technique. The factor was derived for each element by linear regression of the known weight percent of the element in the standards versus their ICP-measured weight percent. These major element data are similar to those that can be acquired by the APXS, ChemCam, and CheMin XRF measurements on Mars.

3.3. Electron Microprobe Analysis

[17] Measurements comparable to electron microprobe analysis are not presently possible on Mars but were performed here on some of the bulk-rock samples to obtain precise compositional data at the mineral grain-scale to verify the identifications made by infrared spectroscopy and XRD. Also, the textural relationships between mineral grains and spatial distribution of alteration (coating versus bulk) could be determined. Rocks were coated in resin to preserve the natural surface during sample preparation, cut, and thin sections of the bulk-rock samples were made. Electron microprobe data were acquired using a Cameca SX 100 instrument with 15 kilovolt acceleration voltage at Brown University. A 15 μm beam diameter and 15 nanoampere beam current were employed to minimize loss due to volatilization of sample components. A combination of optical and backscattered electron data was used to adjust and verify the focus for quantitative measurements of elemental abundance.

3.4. Whole-Rock and Bulk-Rock Infrared Spectroscopy (VNIR, TIR)

[18] In the field and lab, reflectance of whole-rock samples was measured using an Analytical Spectral Devices (ASD) portable VNIR spectrometer over the 0.4–2.5 μm wavelength range, utilizing a contact probe attachment placed on rock faces at different angles. These data are similar to OMEGA or CRISM spectra acquired from Mars orbit, albeit at reduced wavelength range (Figure 2). Additional reflectance spectra of ground pieces of the bulk rock were measured over 0.4–25.0 μm at the Brown University Keck/NASA Reflectance Experiment Laboratory (RELAB) [*Pieters*, 1983], using both a bidirectional spectrometer (measured relative to Halon and calibrated to absolute reflectance) and a Nicolet 740 Fourier-transform spectrometer (measured relative to a rough gold surface in an H_2O- and CO_2-purged environment and calibrated to reflectance). Spectra were examined for broad electronic absorptions, which indicate the presence of minerals with transition metals, most commonly iron, and sharper combination and overtone vibrational absorptions, which indicate the presence of H_2O, metal-OH, and CO_3 [e.g., *Burns*, 1993; *Clark et al.*, 1990].

[19] Whole-rock TIR emission spectra (2000–200 cm^{-1}; 5–50 μm) were acquired using the Arizona State University (ASU) Mars Space Flight Facility thermal emission spectrometer. Samples were heated and maintained at 80°C for the duration of the measurement. A warm and cold blackbody were also measured and used to convert the sample radiance spectrum to emissivity [*Ruff et al.*, 1997]. This procedure produces spectra similar to TES spectra acquired from Mars orbit or MiniTES spectra acquired several meters from an outcrop. Multiple rock faces were measured for some samples including both cut and natural sample surfaces. Spectra were examined for fundamental vibrational absorptions due to Si-O, metal-Si-O, and H_2O. For each spectrum, over the range 1300–300 cm^{-1}, a nonnegative least squares (NNLS) linear unmixing algorithm [e.g., *Rogers and Aharonson*, 2008] was employed using a suite of common igneous and alteration minerals found in the ASU spectral library [*Christensen et al.*, 2000] (Table A1).

3.5. Small-Scale Infrared Spectroscopy (VNIR, TIR)

[20] In addition to orbital and outcrop-scale measurements, microscopic IR instruments have been proposed for in situ investigation of aqueous processes on Mars [e.g., *Grady*, 2006; *Bibring and the Micromega Team*, 2008]. Here, we could not directly simulate these imaging microscopes over the desired wavelength range, so samples were extracted by hand from the bulk rock and individual vesicles and fractures and were measured separately. These were the same particulate samples measured with XRD, and so these analyses also served as a check that grinding and size separation procedures did not result in segregation of mineral phases and a change in sample spectral properties. As above, these particulate samples were measured in the RELAB facility. Over the 5.5–25.0 μm TIR wavelength range, reflectance data were converted to approximate emissivity by Kirchhoff's law (E = 1 − R), an approach that has been shown to yield good agreement with actual emissivity measurements [*Mustard and Hays*, 1997; *Bishop et al.*,

Table 1. Modal Mineralogy of Iceland Samples as Determined by XRD Peak Area Fitting and Rietveld Refinement

		Qualitative Spectrally Determined Mineral/Structural Element		XRD-Determined Mineralogy								
Sample	Description (Figure)	VNIR	TIR	Pyroxene	Plagioclase	Ilmenite	Hematite	Smectite	Cristobalite, Quartz	Quartz	Celadonite	Zeolite
hvalfj011	gray, fiable rock (1d)	HCP + Fe/Mg smectite + (chlorite?)	H_2O-bearing, altered basalt, high silica phase	34	40	5		17				5 (clinoptilolite)
hvalfj017	reddish friable rock (1d)	montmorillonite + hematite	H_2O-bearing, dioctahedral ferruginous smectite		10		10	79				2 (epistilbite)
hvalfj023[a]	blue-green precipitate in vesicle (1f)	celadonite	celadonite		6			20	35		38	1 (mordenite)
hvalfj025	host rock from rock with vesicles with blue-green precipitate (1f)	HCP + hydrated phase (FeOH-bearing?)	H_2O-bearing, altered basalt, nontronite	38	49	1	<1	11				
hvalfj054	host rock from rock with vesicles with whitish precipitates (1g)	HCP + Mg smectite	H_2O-bearing, altered basalt, high silica phase	63	5		5	17				9 (levyne) 1 (stilbite)
hvalfj055[a]	opaque white to cream precipitate in vesicle (1g)	thomsonite (+ other zeolite?)	(thomsonite?)					8				36 (scolecite or mesolite) 30 (thomsonite) 26 (stilbite or stellerite)
hvalfj057[a]	transparent white crystalline precipitate in vesicle (1g)	analcime	analcime					33				55 (analcime) 11 (stilbite or stellerite) 1 mordenite
icel009	massive brown rock with greasy feel (1e)	HCP + Fe/Mg smectite	H_2O-bearing, altered basalt, high silica phase	26	49	1	<1	23				
icel010	massive black rock with greasy feel (1e)	HCP + Fe/Mg smectite	altered basalt	28	49	3		20				
wtrfall016[a]	white precipitate from vein (1g)	hydrated silica	quartz, cristobalite		2				3	91		4 (clinoptilolite)

[a]From vesicle or fracture fill rather than the bulk rock.

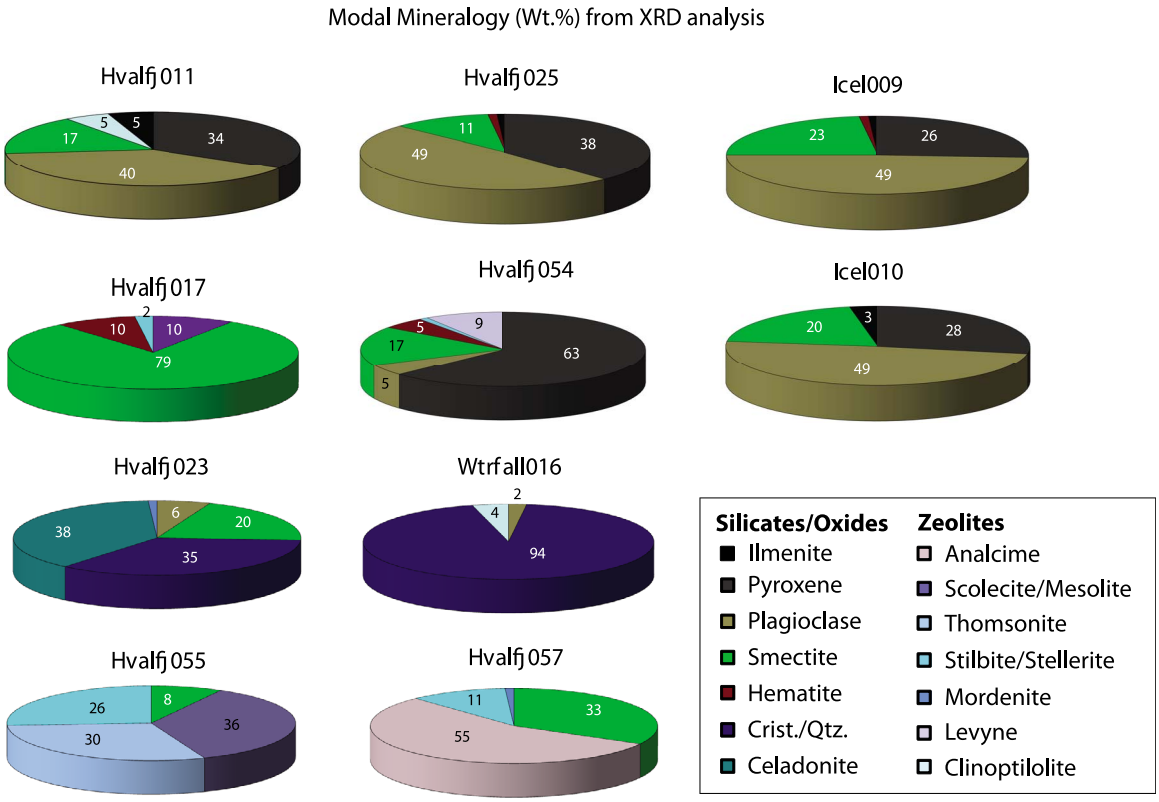

Figure 3. XRD-calculated abundances of minerals or mineral classes for bulk-rock and particulate <25 μm fractions. Data are provided in Table 1 (note: wedges are not labeled for quantities present at ≤1%).

2008b]. The measurement of multiple particle size separates (<25 μm, <150 μm, and 75– or 106–500 μm) over the entire wavelength range permitted evaluation of possible grain size effects on spectral properties. Both VNIR and TIR sample spectra were compared with library spectra for mineral identification. These TIR spectra were not modeled with the linear unmixing routine because the nonlinear volume scattering is significant for particulate samples.

4. Results

4.1. XRD

[21] XRD analyses (Table 1 and Figures 3 and A1) revealed the presence of alteration minerals at from 10 to 80% abundance in all powdered samples.

4.1.1. Bulk-Rock Samples

[22] Hvalfj017 is the most altered of all the samples, containing nearly 80% smectite. Plagioclase and hematite are present at ~10% each, and the zeolite epistilbite is present in small amounts, <5%. Rietveld refinement indicates that the hematite is of very fine crystallite size (~80 nm), and examination of the smectite 060 reflection near $2\theta = 62°$ shows that the smectite present is dioctahedral, e.g., montmorillonite.

[23] Other bulk-rock samples are dominated by the primary mafic components plagioclase and pyroxene (together 65–85%) with hematite and ilmenite <5%. Weight percent smectite ranges from 11 to 23%, and minor amounts of zeolite (<10%) are sometimes present. Hvalfj054 is atypical for its low plagioclase content (5% versus 40–49% for the other bulk rocks) and higher amounts of hematite (5%) and zeolites (10%). The dioctahedral or trioctahedral nature of the smectite in these samples could not be distinguished utilizing the 060 reflection, in part because of overlapping stronger pyroxene and plagioclase reflections.

[24] Modeling of the diffraction patterns of <2 μm size fraction glycolated smectite samples with the NewMod program [*Yuan and Bish*, 2010] shows little to no evidence for interstratification, and the smectite 00*l* basal reflections are consistent with an interstratification of smectite with illite or chlorite at 0–10% levels. The 001 peak for hvalfj025 was broad and asymmetric and appeared to be poorly ordered. It is also possible to estimate octahedral Fe in smectite with NewMod based on the intensity of the 16° 2θ peak, which decreases relatively with increasing iron. Sample hvalfj017 is Fe-poor, sample hvalfj011 has approximately half of its octahedral sites populated with Fe, and hvalfj054 and icel009/010 are relatively Fe-rich.

4.1.2. Vesicle and Fracture Fill

[25] Non-smectite alteration minerals dominate samples extracted from vugs and fractures within the host rocks (Table 1). Hvalfj023 contains ~40% celadonite, a ferrous mica, ~35% cristobalite, and 20% smectite, with minor amounts of Na-rich plagioclase and mordenite. Hvalfj055 and hvalfj057 were sampled from different vesicles within the host rock, separated by a few cm. Hvalfj055 is dominated by a suite of zeolites that includes thomsonite, scolecite or mesolite, and stilbite or stellerite at abundances of 25–35% for each species and smectite (8%) as a minor

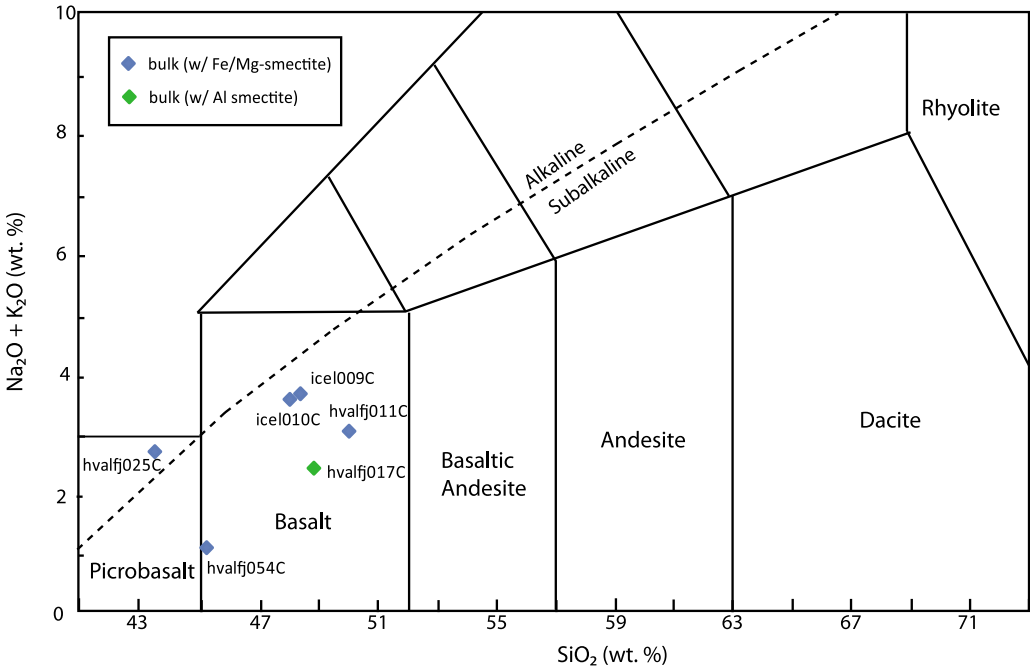

Figure 4. Total alkali-silica diagram for the analyzed samples computed from volatile-free weight percent oxide data.

component. Some of the zeolite minerals are structurally similar and cannot be differentiated without further analyses. More smectite (33%) was found in hvalfj057, which also contains 55% analcime, 11% stilbite or stellerite, and ~1% mordenite. The wtrfall016 sample, from a white precipitate within a fracture, is ~91% quartz and 3% cristobalite along with 2% albite, and <5% clinoptilolite.

4.2. Elemental Analysis

[26] Elemental abundance data, in weight percent oxide, are given in Table A2. Oxide totals ranged from 89.6% to 98.2% with most of the difference from 100% likely due to the presence of H_2O in the samples during measurement. This difference of 2–11% is comparable to that recorded in previous Iceland geochemical analyses [*Franzson et al.*, 2008]. Bulk-rock compositions range from basalt to picrobasalt (Figure 4). Vesicle/fracture fills show different patterns of enrichment/depletion in K (typically mobile), Si, Fe, Al, and Ti (typically immobile) (Figure 5). Wtrfall016 is nearly pure SiO_2, 96%, and low in all other elements. Hvaflj055C and hvalfj057C are enriched in Al_2O_3 with low K_2O and FeO_T. Hvalfj023C, in contrast, has low Al_2O_3, high K_2O, high FeO_T (relative to TiO_2), and high SiO_2. The bulk-rock samples show relatively little compositional variation (Figure 5).

4.3. Microprobe Analysis

[27] Backscattered-electron images combined with quantitative elemental analyses showed that the bulk rocks hvalfj011, hvalfj025, hvalfj054, and icel009 are dominated by plagioclase and pyroxene. Ilmenite (<10% areal fraction) was also found in some samples. Alteration minerals within the samples exhibit textural diversity (Figure 6). Clay minerals occur replacing primary minerals (e.g., pyroxene in Figure 6a), in vesicle fill (e.g., Figure 6e and 6f), and in laths and "worm-like" textures within primary grains (e.g., Figures 6b and 6d). Clay minerals were occasionally associated with iron oxides (e.g., Figures 6c and 6d). In most-altered hvalfj017 (79% smectite, 9% hematite from XRD), nearly all grains exhibit evidence for dissolution or formation of secondary phases. No coatings were observed at a ~5–10 μm scale of probe analysis.

[28] Microprobe quantitative elemental data from individual grains permit analysis of the composition of pyroxenes, feldspars and clay minerals (Figure 7). Compositions of these minerals were computed on the basis of six, eight, and eleven oxygen atoms, respectively. Pyroxenes are high-calcium pyroxenes, falling in the augite field. Two outliers in the ferrosilite field may represent pyroxenes partially altered to smectite. With the exception of two measurements from most-altered sample hvalfj017, all feldspars plot in the plagioclase field with compositions ranging from 0.35 An to 0.95 An. Some of the samples for hvalfj054 have relatively low oxide totals, and may indicate altered feldspar grains. Analyses of very obviously altered grains, filtering to include those with calculated interlayer charge between 0.3 and 0.6, show that smectites are Fe, Mg-smectites, between end-members nontronite and saponite for hvalfj011, hvalfj023, hvalfj054, and icel009. Hvalfj017 smectite has dominantly octahedral Al, e.g., montmorillonite or beidellite composition. Some scatter is exhibited in hvalfj017 and hvalfj023 data, as would be expected with physical mixtures of the alteration phases observed in BSE images at scales less than the 15-μm beam diameter (Figures 6d and 7c). A trend line can be drawn through the data for hvalfj017 that is consistent with mixing of an Al-smectite and hematite. Compositional variability of hvalfj023 clay minerals likely represents mixing between a Fe, Mg smectite and an Fe-rich celadonite (Figures 6e and 7c).

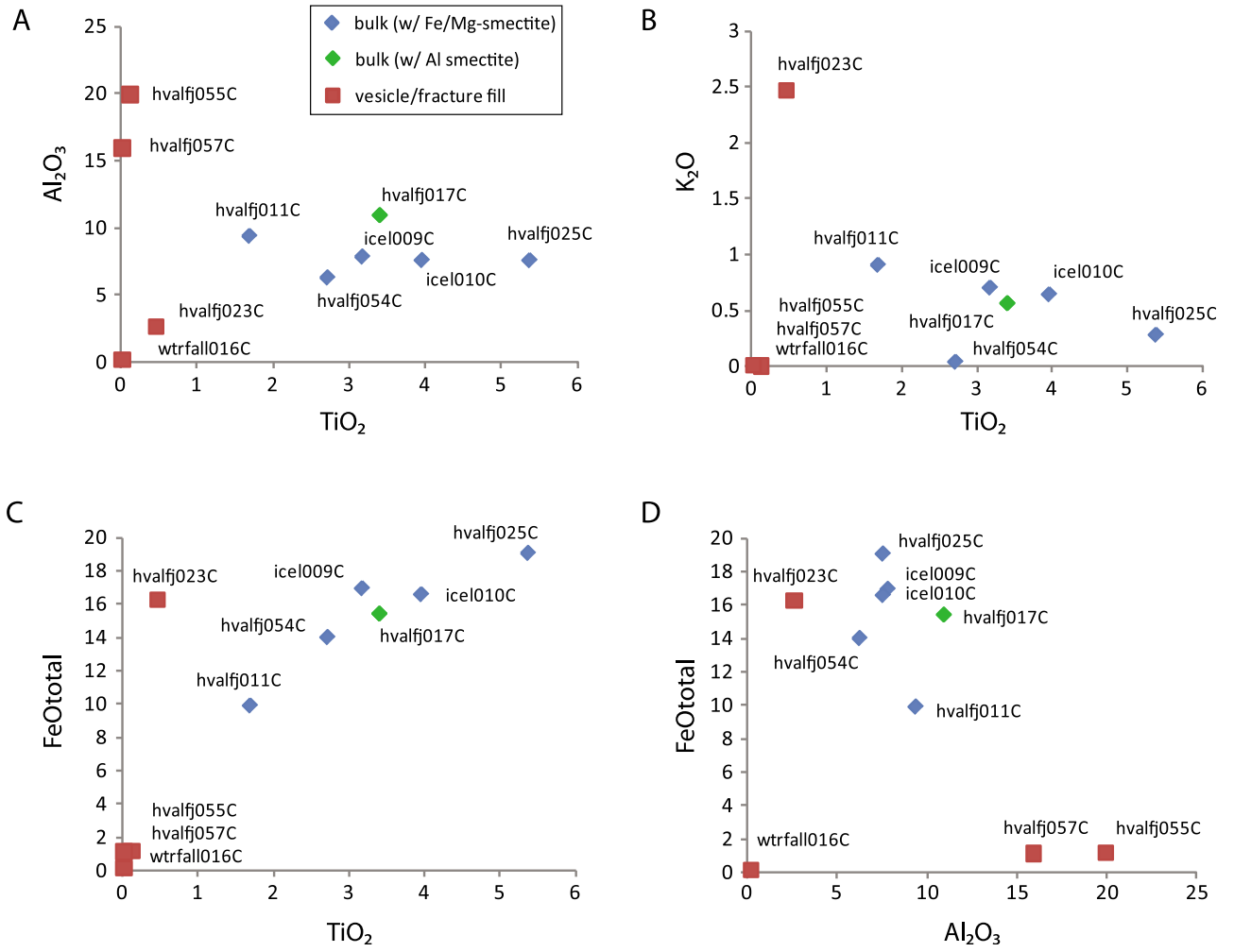

Figure 5. Elemental abundance data in mole versus percent for (a) Al_2O_3 versus TiO_2, (b) K_2O versus TiO_2, (c) FeO_T versus TiO_2 and (c) FeO_T Al_2O_3 showing trends in enrichment and depletion of cations with alteration. Bulk-rock samples show variation in Ti content and correlation between Ti and Fe typical of igneous variability. Fracture fill samples exhibit different styles of alteration.

4.4. Whole-Rock and Bulk-Rock Infrared Spectroscopy

4.4.1. VNIR Spectra

[29] Some of the minerals comprising the sample, usually two or less, can be uniquely identified using the whole-rock and bulk-rock VNIR data (Table 1 and Figures 2 and 8). Hvalfj017 shows absorptions indicating a mixture of hematite and the Al-smectite montmorillonite. Montmorillonite is indicated by an Al-OH band centered at 2.215 μm (8% strength), a 2.44 μm band, and a 2.76 μm Al-OH stretch fundamental (Table 2) [*Bishop et al.*, 1994]. Hematite is indicated by an electronic absorption at 0.86 μm and a charge-transfer absorption at 0.53 μm [*Burns*, 1993]. No absorptions characteristic of pyroxene are present in VNIR data of this sample.

[30] VNIR spectra of five of the six bulk-rock samples show clear absorption features diagnostic of high-calcium pyroxene (HCP) and Fe/Mg smectite (Figure 8a). Pyroxene exhibits broad electronic transition absorptions, centered near 1.0 μm and 2.2 μm for high-calcium pyroxenes such as augite [*Burns*, 1993]. The 1.0-μm band is prominent in these samples. The ~2-μm band is weaker and becomes less prominent as the strength of the 1.9-μm absorption increases (e.g., hvalfj025 versus hvalfj054), an indicator, to first order, of increasing proportion of alteration minerals. The strength of the ~1.9-μm absorption band is related to the amount of H_2O present as H_2O molecules in clay mineral interlayers, in zeolite extra-framework sites, and as surface hydration [e.g., *Bishop et al.*, 1994]. The ~1.9-μm band strength can vary depending on the phases present, relative humidity, thermal history of the hydrated phases, and the nature of the H_2O.

[31] The relative proportions of Fe, Mg, and Al cations in the octahedral sites in smectites dictate the presence and position of absorption bands from 1.35 to 1.45 μm, 2.2–2.3 μm, and near 2.8 μm (Table 2) [*Clark et al.*, 1990; *Bishop et al.*, 2008b]. The 2.3-μm band results from combinations of the 2Fe-OH and 3Mg-OH bending and stretching vibrations, and its position varies depending on the relative proportions of Fe versus Mg in the Fe/Mg smectite series. For example, nontronite, the dioctahedral Fe end-member, has a band center near 2.29 μm [*Grauby et al.*, 1994; *Bishop et al.*, 2002c; *Frost et al.*, 2002; *Gates*, 2005], whereas the trioctahedral Mg end-members saponite

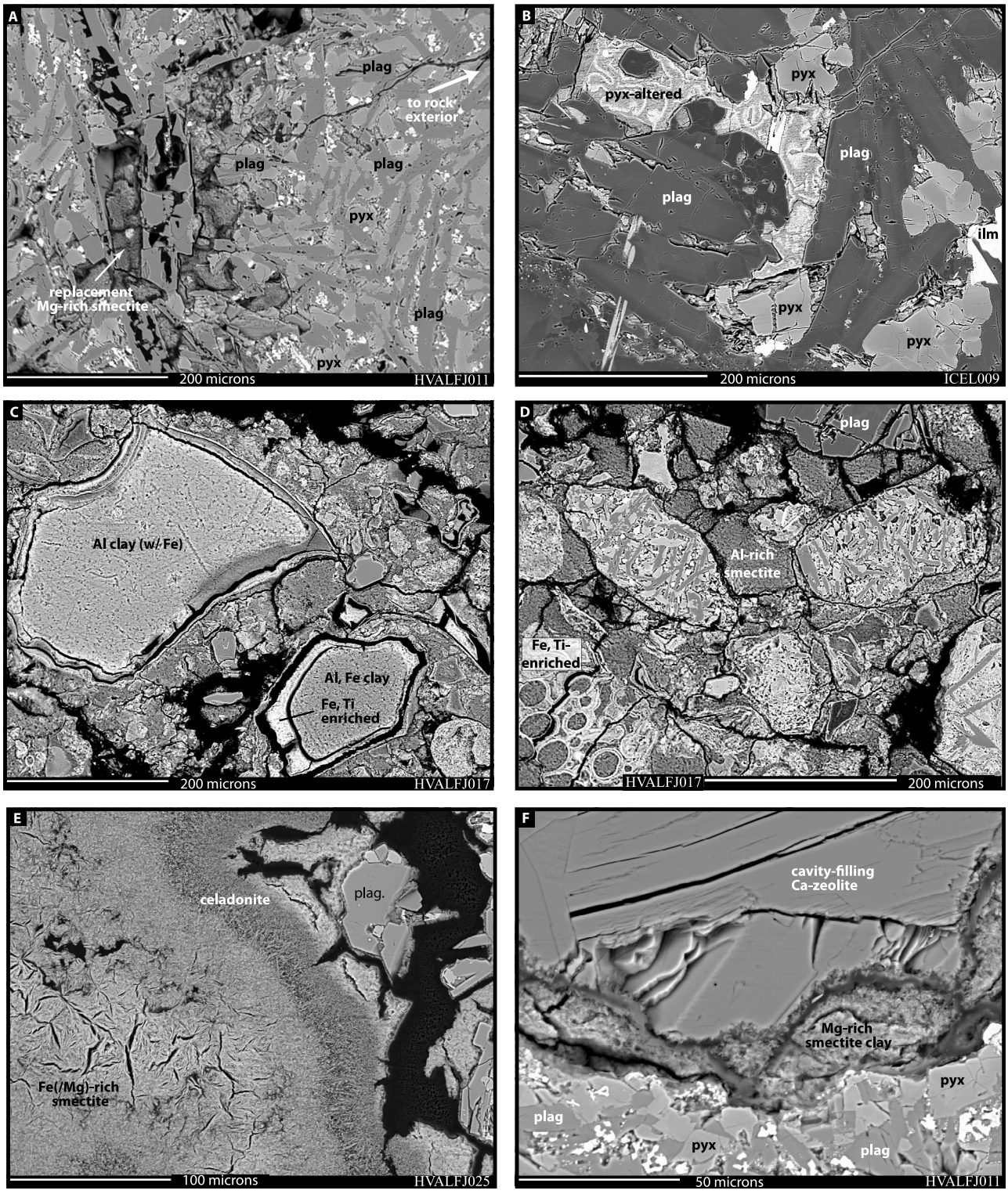

Figure 6. 15 keV backscattered-electron images of alteration styles and textures in samples. (a) Mg-rich smectite replaces pyroxene and plagioclase is dissolved at the interior end of a crack leading from the rock exterior; (b) Fe-rich smectite and Fe-oxides form within a pyroxene grain; (c) almost all primary textures have been replaced and Al-rich smectite clays occur with Fe,Ti-enriched rinds; (d) Same as in Figure 6c except some smectites have an ovoid form; (e) feathery Fe,Mg-rich smectite surrounded by concentric celadonite filling the vesicle; (f) a vesicle filled with Ca-rich zeolite and concentric Mg-rich smectite.

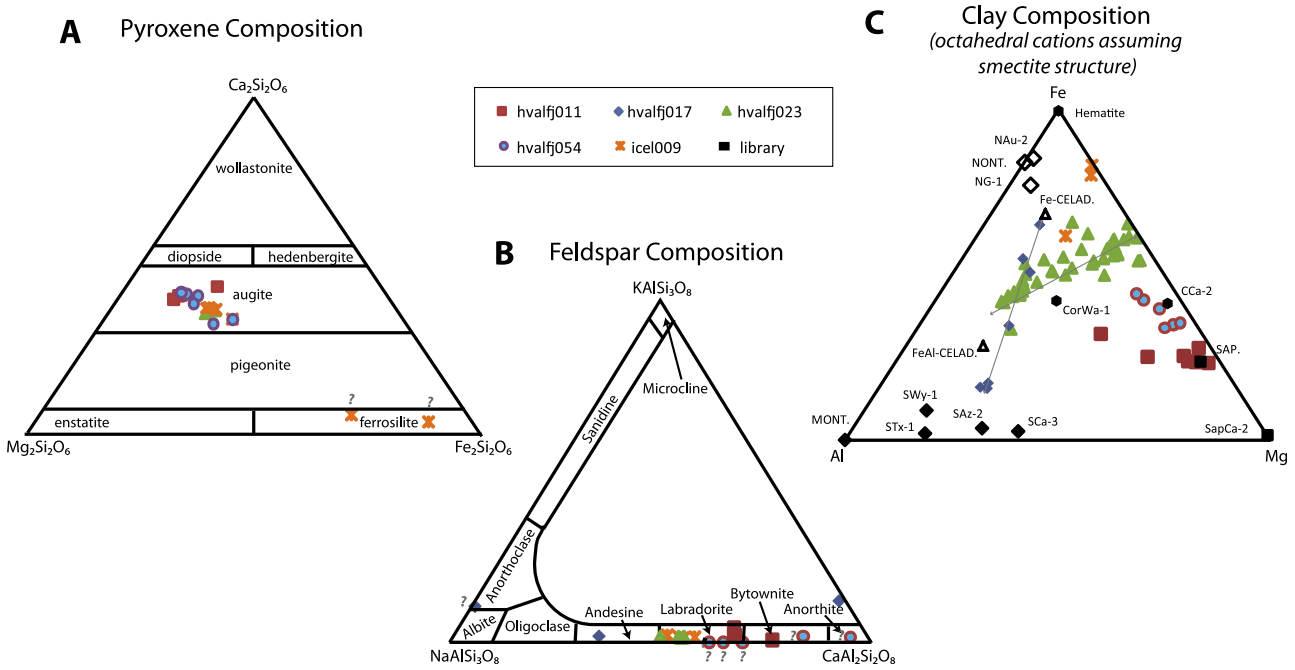

Figure 7. Composition of mineral phases determined by electron microprobe analysis of sample thin sections. (a) Pyroxene compositions plot near augite with the exception of some, possibly altered, grains from icel009. (b) Feldspars from least-altered samples are plagioclases with compositions ranging from 0.35 to 0.95 anorthite. Question marks indicate plagioclases sampled that show textural evidence for alteration and for which the primary composition may not be sampled because electron microprobe oxide totals are <95%. (c) Smectite octahedral cations, computed assuming a smectite structure, show that clays from all samples except hvalfj017 (Al-rich) are consistent with Fe, Mg smectites. Compositional variation in hvalfj017 and hvalfj023 is consistent with physical mixing of smectite with hematite and iron-rich celadonite, respectively. Library clay minerals were computed from elemental compositions of montmorillonite (STx-1, SWy-1, SAz-1, SCa-3), nontronite (NG-1, NAu-2), saponite (SapCa-2), corrensite (CosWa-1), and chlorite (CCa-2) provided by the Clay Minerals Society, clay minerals from MinDat (NONT., MONT., SAP.), and celadonite from *Li et al.* [1997].

and hectorite have absorptions near 2.31–2.32 μm [*Clark et al.*, 1990]. Aluminum, if present in smectite, is indicated by a strong 2.21 μm 2Al-OH combination band [*Bishop et al.*, 2002b, 2008b] (Figure 2a). Combination bands of H_2O are present at 1.41 μm, as is a structural OH stretching overtone that shifts in position, depending on the octahedral cation [*Bishop et al.*, 1994]. This overtone band is at 1.43 μm for 2Fe-OH [*Bishop et al.*, 2002b, 2002c; *Frost et al.*, 2002], at 1.41 for 2Al-OH [*Bishop et al.*, 2002b, 2002c], and at 1.38–1.39 μm for 3Mg-OH [*Clark et al.*, 1990; *Bishop et al.*, 2002b, 2002c]. The fundamental of the metal OH stretch lies at 2.72 μm for Mg-OH, 2.76 μm for Al-OH, and 2.80 μm for Fe-OH [*Grauby et al.*, 1994; *Bishop et al.*, 2002c; *Gates*, 2005] (Figure 8c).

[32] In these Iceland bulk-rock particulate samples, the absorption band depth near 2.3 μm varies in strength from 0.5% (hvalfj025) to 2% (icel009, icel010), much weaker than the combination metal-OH absorption in hvalfj017. Based on the position of the 2.3-μm feature (Figure 8b), most samples are smectites intermediate between the Fe and Mg end-members. Hvalfj025 may be comparatively more iron-rich than icel009 and icel010, based on the band positions at 1.425 and 2.295 μm. Interestingly, all samples have a strong 2.8-μm absorption due to Fe-OH but do not exhibit a prominent 2.76-μm Mg-OH stretch fundamental. Hvalfj011 may be a mixture of multiple smectites as two distinct features due to Fe-OH and Mg-OH are present near 2.3 μm and the Al-OH band is most prominent near 2.76 μm (Figure 8c).

4.4.2. TIR Spectra

[33] Several features of the thermal emission spectra provide information on silicate mineralogy (Figure 9 and Table 2). The Christiansen feature is the emissivity maximum on the short wavelength side of the Si-O stretching minimum that is sensitive to Si-polymerization in framework silicates [*Walter and Salisbury*, 1989]. It occurs between 1150 cm^{-1} (icel009, hvalfj054) and 1300 cm^{-1} (hvalfj025, icel010) in these samples, indicative of the relatively low bulk SiO_2 (silica) of basalts and alteration products. Hvalfj025c ("c" here and in subsequent cases indicates a cut surface), hvalfj011c, and icel010 resemble relatively unaltered basalts, but the other samples lack the broad U-shape or box-like structure (two minima or inflections) in the reststrahlen region on either side of 10 μm (1000 cm^{-1}) that is characteristic of unaltered basalts. Instead they have a shape more typical of andesites, altered basalts, or high-silica glasses [*Wyatt et al.*, 2001; *Wyatt and McSween*, 2002]. The notably narrow V-shape and low wave number of this feature for samples hvalfj011n ("n" here and in subsequent cases indicates a natural surface), hvalfj017n and c,

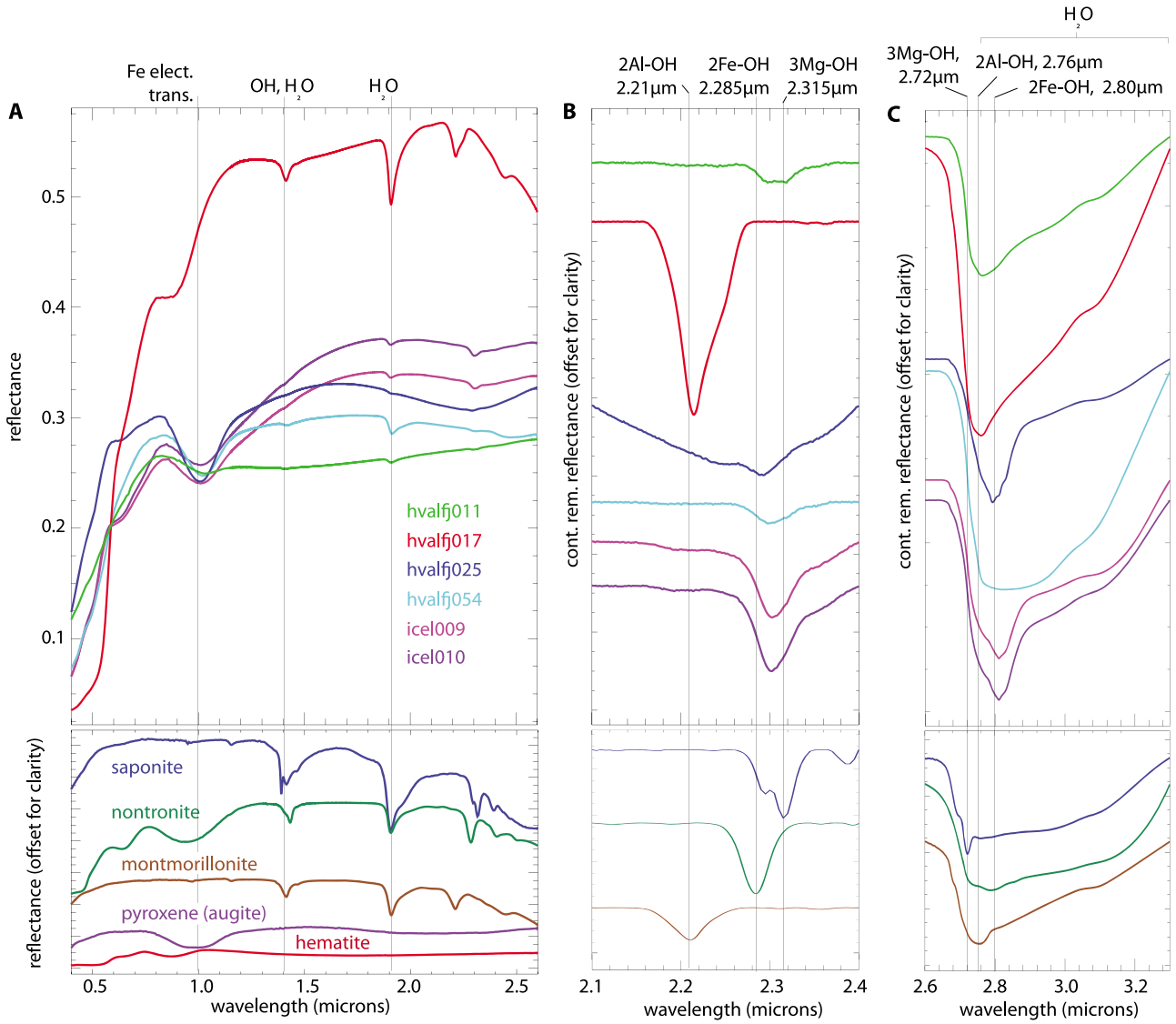

Figure 8. Bidirectional visible near-infrared (VNIR) reflectance spectra for the <25 μm particle size separates from bulk-rock samples measured with XRD. (a) Major absorption features can be discerned and compared with library spectra over the 0.4–2.6 μm region, identifying smectites, pyroxene, and hematite. (b) Metal-OH related combination ($\nu + \delta$) vibrational absorptions and (c) stretching (ν) fundamentals.

Table 2. Positions of Features Related to Hydrated Silicates (e.g., Clay Minerals) in Samples From the Bulk Rock Compared With Band Centers for End-Member Smectite Compositions[a]

Sample	$2\nu_{OH}$ (μm)	$\nu_{OH} + \delta_{m\text{-}OH}$ (μm)	$2\nu_{OH}$ (μm)	$\nu_{Si\text{-}O}$ (cm^{-1})	$\delta_{(Al,Si)\text{-}Si\text{-}O}$ (cm^{-1})
hvalfj011	1.415	2.297, 2.319	2.76	1038	527sh, 472
hvalfj017	1.415	2.215	2.76	1045	520, 466
hvalfj025	1.425	2.293	2.792	1061	519, 448
hvalfj054	1.42	2.298	(broad)	1042–1034	538sh, 460
icel009	1.410, 1.440	2.302	2.81	1053, 987	500, 453
icel010	1.410, 1.440	2.302	2.81	1185, 1024	–
Nontronite	1.43	2.28–2.29	2.80	1056–1068	510–515, 455–440
Saponite	1.38–1.39	2.31–2.32	2.72	1037	475–480
Montmorillonite	1.41	2.21	2.76	1055–1070 (1137)	525–535, 470–475

[a]Band centers were determined from continuum removed spectral data.

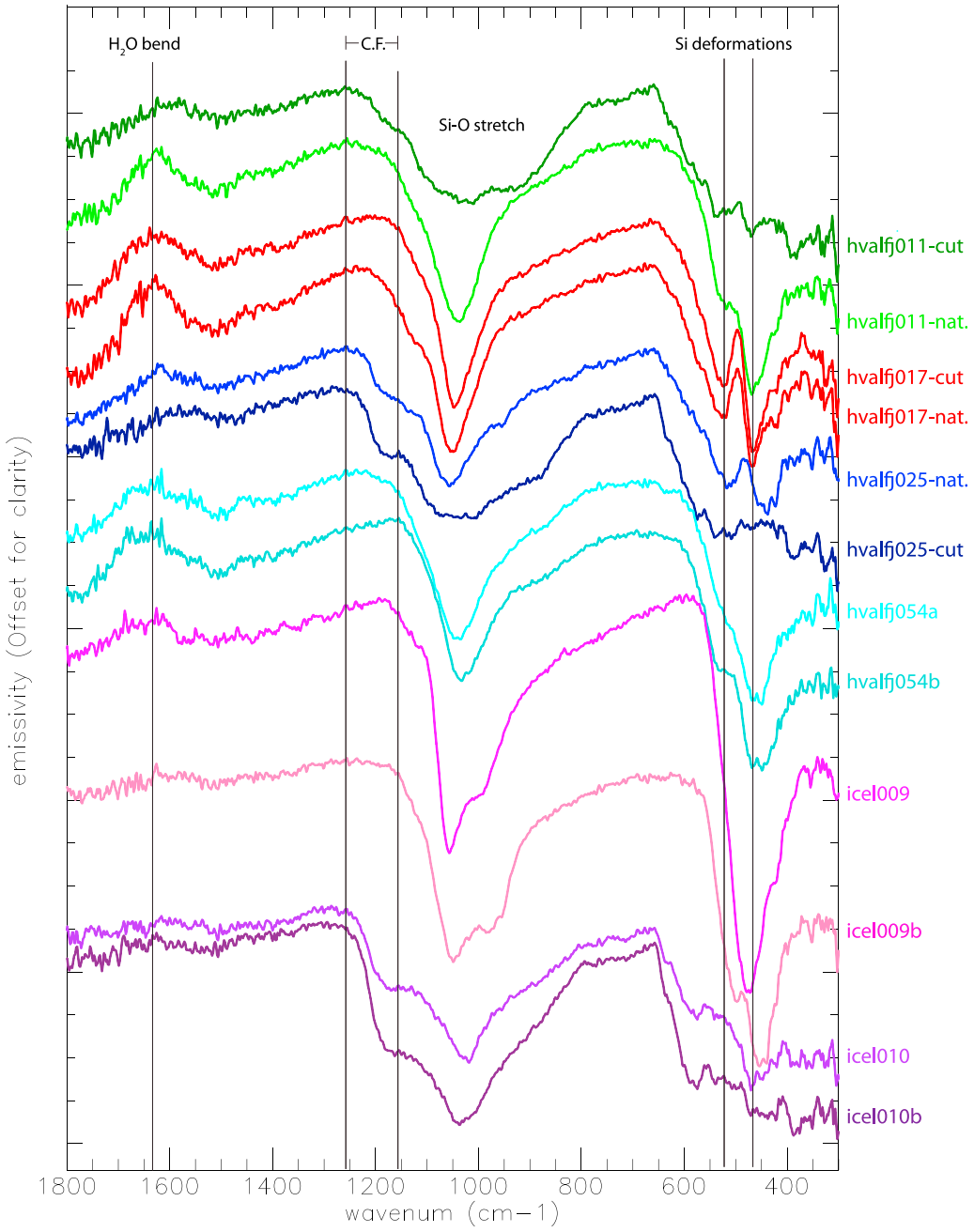

Figure 9. Thermal infrared (TIR) emission data for all whole-rock samples. The H_2O bending fundamental is present in most samples, and the Christiansen feature (CF), Si-O stretch, and deformation bands are diagnostic of degree of alteration and composition. Two faces of each rock are shown, indicated by *n* and *c* for natural and cut surfaces or simply *a* and *b* for two different natural surfaces.

hvalfj054, and icel009 are most consistent with various phyllosilicates [*Michalski et al.*, 2005].

[34] All rock samples except icel010 exhibit a 6-μm (1625 cm^{-1}) peak due to the H_2O bending fundamental, indicating the presence of minerals with H_2O [e.g., *Salisbury et al.*, 1991] (Figure 9). Relatively weak features due to metal-OH bands in clay minerals occur from 750 to 950 cm^{-1} [*Michalski et al.*, 2005] but are not observed in these rocks. Minima observed near 530 cm^{-1} and 465 cm^{-1} (Figure 5a) are caused by vibrations due to metal-O-Si and Si-O-Si deformations with the positions of the bands shifting depending on the metal cation (Al, Fe, Mg) and mineral structure [*Bishop et al.*, 2002b; *Michalski et al.*, 2005, and references therein]. These features occur paired or singly in clays and zeolites and have been used in mapping of alteration minerals, including zeolite and smectites, on Mars [e.g., *Ruff and Christensen*, 2007]. The presence of a spectral doublet (paired features) in this region is a strong indication of dioctahedral smectites. In hvalfj017 for example, minima positioned at 525 cm^{-1} and 463 cm^{-1} closely match those of a library dioctahedral ferruginous smectite and are near montmorillonite (Table 2) [*Bishop et al.*, 2008b;

Michalski et al., 2005]. Hvalfj025n exhibits a doublet with features at 513 cm^{-1} and 440 cm^{-1}, positions that closely match features expected for nontronite (NAu-2) [*Michalski et al.*, 2005]. Rocks hvalfj054 and hvalfj011n exhibit a prominent Si-O-Si deformation feature at 463 cm^{-1} but have a weak shoulder at the Al-O-Si deformation at 530 cm^{-1} rather than a well-developed minimum. This is suggestive of a dominant trioctahdral smectite perhaps with a lesser dioctahedral component. Depending on which face is observed, icel009 has a very strong single minimum at 470 cm^{-1} or a doublet at 496 cm^{-1} and 447 cm^{-1} along with unusual features in the 1000 cm^{-1} region that are not readily interpretable. Cut surfaces of hvalfj011 and hvalfj025 have reduced to absent deformation bands compared to their natural surfaces, while those in hvalfj017 do not change from the cut to natural surfaces, demonstrating that some of the samples have spectrally distinct exteriors and some do not (Figure 9).

[35] The nonnegative least squares modeling (unmixing) of the TIR emissivity spectra (Figure 10) shows a range of results that are a function of the available spectral library and the physical characteristics of the samples. Note that the high wave number cutoff used in the modeling was chosen to avoid a pronounced downturn or roll-off in emissivity present in most of the spectra above 1300 cm^{-1}. This characteristic is typically associated with scattering effects from fine particulates that create so-called transparency features [e.g., *Salisbury and Eastes*, 1985]. Its appearance in the spectra of whole rocks suggests a comparable scattering phenomenon. Because the library spectra do not show this behavior in the region >1300 cm^{-1}, the modeling excluded it.

[36] Hydrated silicates (phyllosilicates, zeolites) were modeled in all the rocks, with abundances ranging from 17% (icel010b) to 86% (hvalfj017n) (Figure 10 and Table 3). Feldspars dominated by plagioclase compositions range from 0% (hvalfj011n, hvalfj017n and c, hvalfj054a and b, icel009a and b) to 49% (icel010b). Pyroxenes range from 0% (hvalfj011n, hvalfj017n and c, hvalfj054a and b, icel009a and b, icel010a) to 15% (hvalfj025n). Olivines range from 2.5% (hvalfj017) to 19% (hvalfj011).

4.5. Small-Scale Infrared Spectroscopy (VNIR, TIR)

4.5.1. VNIR Spectra

[37] Only single minerals could be identified from VNIR data of samples extracted from rock veins and vesicles (Table 1). Hvalfj023 appears to contain the dioctahedral mica celadonite, with characteristic absorptions of approximately equal strength at 2.30 μm ($2Fe^{3+}OH$ combination) and 2.35 μm (3MgOH combination) and strong slope to 1.0 μm (Figure 11a). A weaker absorption can also be seen at 2.26 μm due to an $AlFe^{3+}OH$ combination [*Bishop et al.*, 2008b].

[38] NIR spectral features of zeolites are dominated by absorptions from H_2O molecules [*Hunt et al.*, 1973; *Clark et al.*, 1990], and zeolites, which have H_2O molecules in extraframework sites, are the likely source of relatively deep 1.4 and 1.9 μm features in hvalfj055 and hvalfj057 (Figure 11b). In some cases, due to their different structures and cations, zeolites have distinctive absorptions that permit discrimination among individual phases [*Clark et al.*, 1990; *Cloutis et al.*, 2002]. Hvalfj057 contains analcime, which is characterized by strong absorptions at 1.42 μm, 1.91 μm, 2.52 μm and weaker absorptions at 1.79 μm, 1.12 μm, 2.14 μm. Sample hvalfj055 contains thomsonite, distinguished by a small feature at 2.17 μm. There is also a 2.4 μm feature in the sample that is not characteristic of thomsonite but is typical of many other zeolites or other hydrated mineral phases [*Cloutis et al.*, 2002].

[39] Finally, sample wtrfall016 has spectral features consistent with hydrated silica (Figure 11c). Opaline silica and hydrated (H_2O-bearing), hydroxylated (OH-bearing) glasses exhibit absorption bands due to combination bands of Si-OH at 2.21–2.22 μm due to isolated Si-OH and at 2.26 μm due to H-bonding with Si-OH [*Anderson and Wickersheim*, 1964; *Stolper*, 1982; *Goryniuk et al.*, 2004]. The width of the resultant feature near 2.2 μm is greater than the Al-OH absorption in aluminum phyllosilicates [*Milliken et al.*, 2008]. Bands at 1.91 μm are due to H_2O in the mineral structure whereas those near 1.4 μm result from both H_2O and structural OH. The 1.4 and 2.3 μm, absorptions can become narrow as H_2O is removed and only Si-OH remains [*Anderson and Wickersheim*, 1964; *Swayze et al.*, 2007; *Milliken et al.*, 2008], but the bands in this sample are broad, indicating incorporation of H_2O in the silica structure.

4.5.2. TIR Spectra

[40] The infrared reflectance spectra of separates of the bulk-rock samples are influenced by particle size (Figure 11d). There is a broad transparency feature above ~1300 cm^{-1} in the finer-grained samples (<150 μm) that arises from fine-particulate scattering as described previously, as does the narrower feature between ~1000 and 800 cm^{-1} in samples hvalfj023C, 055C, and 057C and D. The pronounced particle-size induced roll-off at high wave numbers tends to accentuate the appearance of the H_2O bending fundamental near 6 μm, indicating the presence of bound H_2O in samples hvalfj023, 055, and 057.

[41] Particle size separate spectra of hvalfj023 exhibit some of the characteristics of library celadonite samples [*Bishop et al.*, 2008b] (RELAB database) although with deviations that suggest an incomplete match (Figure 11d). Hvalfj057 shows all of the features found in the laboratory analcime [*Ruff*, 2004; *Clark et al.*, 2007] while hvalfj055 [*Cloutis et al.*, 2002] appears to be a better match to thomsonite. The wtrfall016 sample clearly exhibits the typical absorption features of quartz [*Farmer*, 1974] but with an asymmetry possibly due to cristobalite [*Michalski et al.*, 2003].

5. Discussion

[42] Results from both spectroscopy and XRD indicate that the dominant alteration mineral in bulk-rock samples is smectite clay with only minor amounts of other hydrated silicates. In contrast, for samples extracted from veins and vesicles, hydrous silicates other than smectite are the dominant alteration mineral(s), e.g., zeolites, SiO_2 phases, and other phyllosilicates.

5.1. Chemical Versus Mineralogical Analyses of Alteration

[43] Based on elemental chemistry, the Icelandic bulk-rock samples are basalts or picrobasalts (Figure 4), though evidence from VNIR, TIR, and XRD techniques indicates these rocks have been altered. The extent and nature of alteration varies substantially by sample. For most of the bulk-rock samples (hvalfj011, hvalfj025, hvalfj054, icel009,

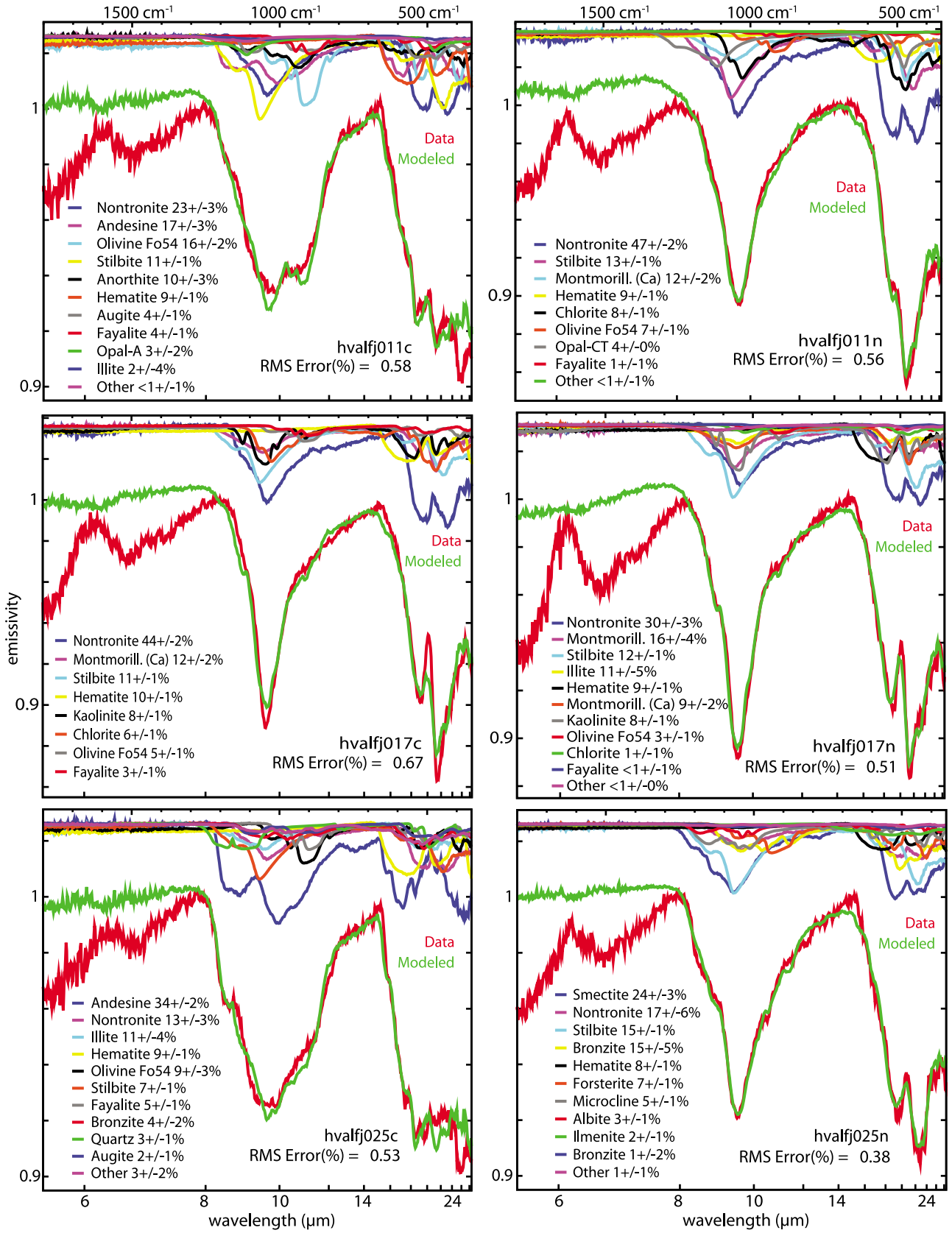

Figure 10. Nonnegative least squares fits of model TIR emission spectra to measured spectra for the 12 bulk-rock samples. The letters *n* and *c*, indicate natural and cut surfaces, respectively, or simply *a* and *b* for two different natural surfaces. Phases with abundances modeled at >2% are plotted.

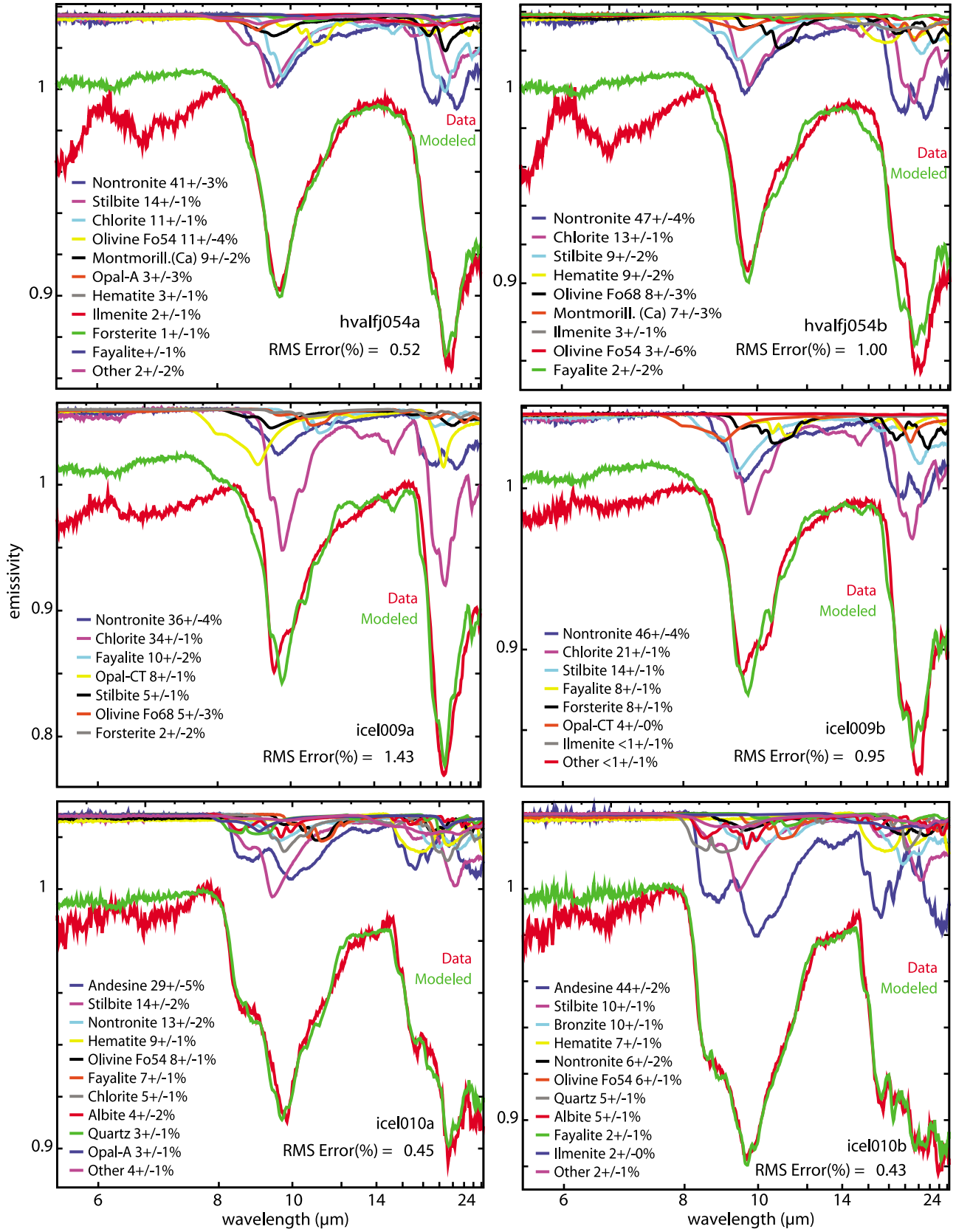

Figure 10. (continued)

Table 3. TIR Modeled Abundances, for Components at >2% Level[a]

	hvalfj011c	hvalfj011n	hvalfj017c	hvalfj017n	hvalfj025c	hvalfj025n	hvalfj054a	hvalfj054b	icel009a	icel009b	icel010a	icel010b
Smectite	23 ± 3 (nont.)	47 ± 2 (nont.) 12 ± 2 (mont.)	44 ± 2 (nont.) 12 ± 2 (mont.)	30 ± 3 (nont.) 25 ± 7 (mont.)	13 ± 3 (nont.)	24 ± 3 (Swa-1) 17 ± 6 (nont.)	41 ± 3 (nont.) 9 ± 2 (mont.)	47 ± 4 (nont.) 7 ± 3 (mont.)	36 ± 4 (nont.)	46 ± 4 (nont.)	13 ± 2 (nont.)	6 ± 3 (nont.)
Other hyd. silicate		8 ± 1 (chl.)	8 ± 1 (kaol.) 6 ± 1 (chl.)	11 ± 5 (illite) 8 ± 1 (kaol.)	11 ± 4 (illite)		11 ± 1 (chl.)	13 ± 1 (chl.)	33 ± 1 (chl.)	21 ± 1 (chl.)	6 ± 1 (chl.)	
Zeolite		13 ± 1 (stilbite)	11 ± 1 (stilbite)	12 ± 1 (stilbite)	7 ± 1 (stilbite)	15 ± 1 (stilbite)	15 ± 1 (stilbite)	9 ± 2 (stilbite)	5 ± 2 (stilbite)	14 ± 1 (stilbite)	14 ± 2 (stilbite)	10 ± 1 (stilbite)
Silica	3 ± 2 (opal-A)	4 ± 1 (opal-CT)			3 ± 1 (qtz.)		3 ± 3 (opal-A)		8 ± 1 (opal-CT)	4 ± 1 (opal-CT)	3 ± 1 (qtz.) 3 ± 1 (opal-A)	4.9 ± 1 (qtz.)
Hematite	9 ± 1	9 ± 1	10 ± 1	9 ± 1	10 ± 1	8 ± 1	3 ± 1	9 ± 2			9 ± 1	7 ± 1
Plagioclase	17 ± 3 (andes.) 10 ± 3 (anorth.)				34 ± 2 (andesine)	5 ± 1 (microcline) 3 ± 1 (albite)					29 ± 5 (andesine) 4 ± 2 (albite)	44 ± 2 (andesine) 5 ± 1 (albite)
Pyroxene	4 ± 1 (augite)				4 ± 2 (bronzite) 2 ± 2 (augite)	15 ± 5 (bronzite)						10 ± 1 (bronzite)
Olivine	16 ± 2 (Fo54) 4 ± 1 (fay.)	7 ± 1 (Fo54)	5 ± 1 (Fo54) 3 ± 1 (fay.)	3 ± 1 (Fo54)	9 ± 3 (Fo54) 5 ± 1 (fay.)	7 ± 1 (for.)	11 ± 4 (Fo54)	8 ± 3 (Fo68) 3 ± 6 (Fo54)	10 ± 2 (fay.) 5 ± 3 (Fo68) 2 ± 2 (for.)	8 ± 1 (fay.) 8 ± 1 (for.)	8 ± 1 (Fo54) 7 ± 1 (fay.)	6 ± 1 (Fo54) 3 ± 1 (fay.)
Ilmenite						2 ± 1	2 ± 1	3 ± 1			3 ± 1	

[a]Abbreviations: nont. = nontronite, chl. = chlorites, andes. = andesine feldspar, anoth. = anorthosite feldspar, Fo = forsterite (where the number signifies the magnesium number); fay. = fayalite, kaol. = kaolinite, qtz. = quartz, for. = forsterite

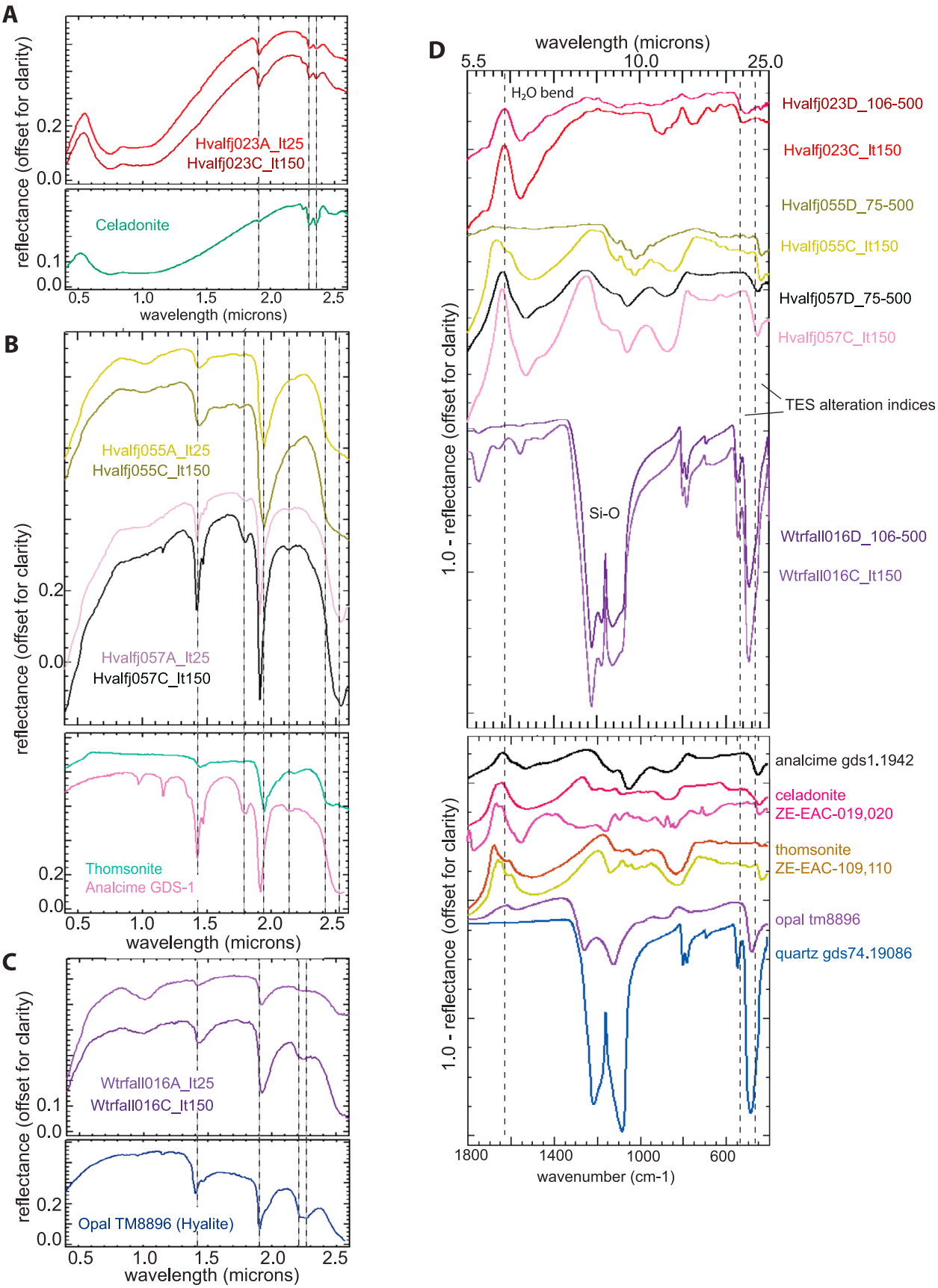
A
reflectance (offset for clarity)
Hvalfj023A_lt25
Hvalfj023C_lt150
Celadonite
wavelength (microns)
B
Hvalfj055A_lt25
Hvalfj055C_lt150
Hvalfj057A_lt25
Hvalfj057C_lt150
Thomsonite
Analcime GDS-1
C
Wtrfall016A_lt25
Wtrfall016C_lt150
Opal TM8896 (Hyalite)
D
wavelength (microns)
H2O bend
Hvalfj023D_106-500
Hvalfj023C_lt150
Hvalfj055D_75-500
Hvalfj055C_lt150
Hvalfj057D_75-500
Hvalfj057C_lt150
TES alteration indices
Si-O
Wtrfall016D_106-500
Wtrfall016C_lt150
1.0 - reflectance (offset for clarity)
analcime gds1.1942
celadonite
ZE-EAC-019,020
thomsonite
ZE-EAC-109,110
opal tm8896
quartz gds74.19086
wavenumber (cm-1)

Figure 11

and icel010), the primary mafic minerals pyroxene and plagioclase still comprise most of the sample; alteration minerals are <25 wt. % and are mostly Fe, Mg smectites (Figure 3). Nevertheless, hydration bands are prominent in VNIR spectra and nearly all TIR spectra. Smectites are found within and surrounding grains of primary mafic minerals, i.e., comprising the bulk rock, and IR spectral signatures from bulk rocks samples exhibit features related to the presence of smectite clays (Figure 6). The persistence of crystalline igneous minerals is similar to that found in deeper, higher temperature Iceland drill cores from seawater hydrothermal systems [*Marks et al.*, 2010].

[44] The vugs and fractures of the rocks have concentrated zeolites, celadonite, and silica phases rather than phyllosilicates, but in the bulk rock separates these phases occur in <10% abundance and are not identifiable at VNIR wavelengths (Table 1 and Figure 8). Based on the trends of Al, K, and Fe content relative to comparatively immobile Ti in materials filling vugs and fractures, it is clear that different fluid chemistries or thermodynamic conditions variously favored transport and then precipitation and enrichment of K and Fe together (hvalfj023), enrichment of Al and Si (hvalfj057, hvalfj055), or enrichment of Si only (wtrfall016) relative to the bulk rock (Figure 5). Such differences have also been reported in other Icelandic groundwater and hydrothermal systems [*Franzson et al.*, 2008].

[45] Bulk-rock sample hvalfj017 is distinctive in its high percentage (89%) of alteration minerals, specifically hematite and montmorillonite (Figure 3 smf Table 1). The different mineralogy points to a distinctive alteration history relative to the other bulk samples. Hvalfj017 was found at the boundary between two flows (Figure 1d) and may represent the uppermost surface of a lava flow in which paleosol development occurred prior to emplacement and burial by the second flow. Alternatively, the reddish zone at the flow boundary from which hvalfj017 was derived may have been a concentrated pathway of fluid flow with consequently more intense water-rock interaction.

[46] Interestingly, bulk-rock samples all plot similarly in chemical diagrams in spite of different proportions of alteration minerals and, presumably, different amounts of removal and addition of ions by interaction with fluids. The most-altered bulk-rock sample in terms of mineralogy, hvalfj017, does not differ from less altered samples, suggesting the alteration may have been nearly isochemical with only small-scale chemical transport and mineralization in vesicles (Figures 4 and 5). In a ternary plot of major cations, which has been used to study weathering trends in Mars samples (Figure 12) [*Hurowitz and McLennan*, 2007], even for the 80% smectite hvalfj017 with its nearly complete lack of primary minerals, there is little progression along the typical terrestrial weathering trend toward the Al vertex. Most of the variation lies along the feldspar-olivine join with alteration products filling veins and vesicles and becoming either Fe-enriched or Fe-depleted. Variation along this line was also typical for low water:rock ratio acidic alteration on Mars [*Hurowitz and McLennan*, 2007]. For these Icelandic environments of alteration, whole-rock elemental analyses might lead to underestimation of the extent of alteration relative to the higher degree apparent from XRD-derived quantitative modal mineralogy or VNIR or TIR spectroscopy. Although alteration is extensive in some cases, changes in a whole-rock sense are largely isochemical in these samples, demonstrating the importance of knowledge of mineralogy in addition to chemistry in the exploration of Mars. One hypothesis is that Mars' large Fe, Mg clay-bearing terrains might be a result of aqueous alteration, similar to that observed in these Icelandic systems, with primary minerals dominating assemblages with Fe, Mg clays and little chemical fractionation and transport, thus explaining lack of chemical fraction in orbital GRS data [*Ehlmann et al.*, 2011a]. Future tests will await landed or next-generation orbital measurements.

5.2. Mineral Identification With VNIR and TIR Spectroscopy

[47] Spectroscopic techniques, comparable to remote measurements from Mars orbit, provide a good first means of characterization of mineralogy. No misidentifications were made with VNIR data; all Al smectite, hematite, Fe, Mg smectite, high calcium pyroxene, zeolite, silica, and celadonite phases identified from VNIR spectroscopy (Table 1) were confirmed by XRD, although the actual mineral assemblage revealed by XRD typically is more diverse (Table 1). Plagioclase cannot be directly detected in VNIR spectra because it possesses neither electronic absorptions due to Fe nor vibrational absorptions in the VNIR wavelength range. Zeolites at <10% abundance occurring in the bulk rock were not detected with VNIR spectroscopy because they enhance the 1.9-μm H_2O combination absorption, typically without introducing strong diagnostic additional bands in the wavelength region from 2.0 to 2.6 μm [*Cloutis et al.*, 2002]. The presence of some alteration minerals spectroscopically masks the presence of others. For example, analcime and celadonite in hvalfj057 and hvalfj023, respectively, obscure 33 wt. % and 20 wt. % of XRD-identified smectite in VNIR data (Table 1). The presence of celadonite (38 wt. %) in hvalfj023 masks cristobalite (35 wt. %) in VNIR data.

[48] TIR spectroscopy also indicates several key aspects of the mineralogic composition, including the presence of hydrated minerals in all samples. Like VNIR spectroscopy, small-scale TIR spectroscopy identifies the major phase for each fracture/vesicle fill sample. Visual inspection of 600–400 cm^{-1} minima positions in whole-rock samples hvalfj017 and hvalfj025 correctly identified montmorillonite and nontronite, respectively, as the dominant smectite in each sample (Table 2 and section 4.4.2) although quantitative modeling

Figure 11. (a–c) Bidirectional visible near-infrared (VNIR) reflectance spectra for the <25 μm and <150 μm particle size separates from veins and fracture fill (Figure 1). (d) TIR reflectance spectra of coarse (75 or 105–500 μm) and <150 μm size fractions of the vesicle and fracture fill samples, converted to approximate emission spectra using Kirchhoff's law. Positions of key absorptions are indicated. Laboratory spectra provided for comparison are from the USGS spectral library [*Clark et al.*, 2007] and as acquired by E. Cloutis at the NASA RELAB facility at Brown University.

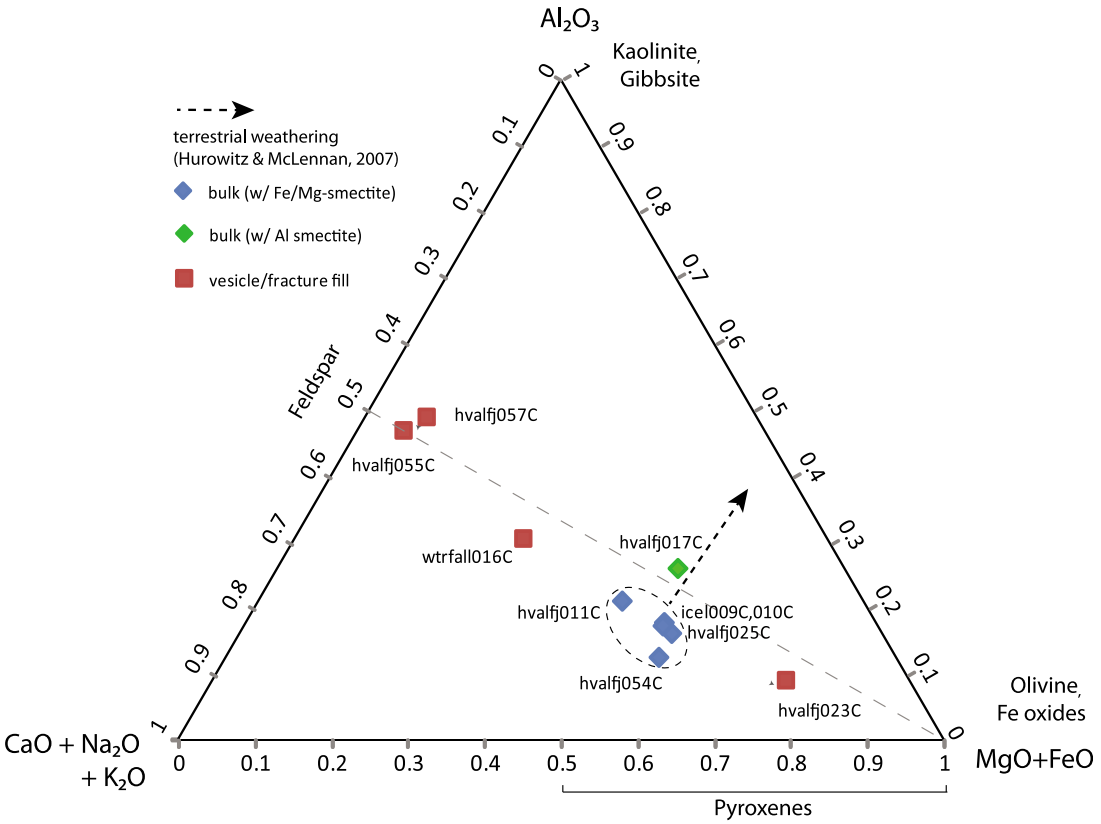

Figure 12. Ternary Al_2O_3, ($CaO + Na_2O + K_2O$), (FeO_T + MgO) diagram, data plotted in mole percent. The bold black arrow indicates the direction of terrestrial weathering [after *Hurowitz and McLennan*, 2007]. Light gray arrows indicate relationships between bulk rocks (blue diamonds for Fe/Mg smectite-bearing, green diamonds for Al smectite-bearing) and vesicle/fracture fill (orange squares) found within those bulk rocks.

was less successful in accurately identifying phases present (discussed below). For these particular samples, the Christiansen feature did not provide a good indicator of overall SiO_2 content (Figure 4 versus Table A1), likely due to the effects of alteration on disrupting polymerization of silicates as has been reported in other studies [*Hamilton et al.*, 2008].

[49] Two interesting aspects of silica and clay mineral identification with spectroscopy, relevant to interpretation of remotely sensed data, relate to the different types of information obtainable in the combination band wavelength region versus the fundamental stretch region. First, VNIR spectra of wtrfall016 show that a silica phase is present, and it is consistent with a hydrated Si-OH phase, e.g., opaline silica or altered glass (Figure 11). TIR spectra are consistent with quartz and cristobalite and the XRD data unambiguously demonstrate the existence of quartz (91%) and cristobalite (3.3%), with minor clinoptilolite (3.9%) and no evidence for a significant amount of an amorphous component (Figures 3 and 11 and Table 1). That quartz or cristobalite can have a similar VNIR spectral signature to opaline silica may have implications for reconciling reports of hydrated opaline phases [*Milliken et al.*, 2008; *Ehlmann et al.*, 2009] and quartz [*Bandfield et al.*, 2004] on Mars.

[50] Second, the OH stretch fundamentals (near 3 μm) appear to be less diagnostic of the major smectite cation than the combination tones from 2.20 to 2.35 μm. In the 2.2–2.3 μm region, Al-OH, Fe-OH and Mg-OH related bands can be observed (Figures 2 and 8b) that shift in accordance with smectite composition (Figure 7c). In particular, that hvalfj011 is an Mg-rich smectite, hvalfj025 an Fe-rich smectite, and hvalfj017 an Al-rich smectite can be discerned. Although chemical data show that all of the bulk rocks (except hvalfj017) have both Fe and Mg in octahedral sites (Figure 7c), spectra show only fundamentals at wavelengths for Fe-OH and Al-OH (Figure 8c). Lack of resolution of an Mg-OH band may be due to the influence of H_2O on the spectra from 2.7 to 3.0 μm [e.g., *Gates*, 2005]. Deformation bands positioned at 400–600 cm^{-1} permit identification of dioctahedral versus trioctahedral smectite for two of six rocks where a dioctahedral smectite dominates (hvalfj017 and hvalfj025n) and a doublet feature is apparent. Among the other samples, smectite features are not readily apparent (icel010, hvalfj0011c, hvalfj025c) or absorptions in the 400–600 cm^{-1} region do not occur in locations corresponding to those of smectite compositions measured for spectral libraries. These data suggest that existing spectral libraries used in the analysis of Mars data may only incompletely sample the diversity of phases formed from aqueous alteration of basalt.

5.3. A Role for Thin (<10 μm) Surface Coatings?

[51] VNIR whole-rock surface spectra exhibited heterogeneity, depending on the spot of the rock observed (Figure 2), but no systematic differences between cut and natural surfaces. OH-vibrational absorptions due to smectites ranged in strength from strong to barely discernible, although H_2O-related absorptions were always present. Bulk-rock powders exhibited similar variation with band strength of OH features correlated to XRD measured smectite abundances. On the other hand, TIR spectra exhibit systematic variation between cut and natural surfaces. The restrahahlen bands of all the natural rock surfaces have a markedly Si-rich character, and natural surfaces also have bending vibrations due to hydrated silicates. These features are weak or indiscernible for the cut surfaces in two of the three cut samples (hvalfj011 and 025) and for both the natural and cut surfaces of icel010, and H_2O-bending features are weaker in these samples. This suggests the presence of very thin coatings that are not evident in the BSE microprobe images but are evident as discoloration of the natural surfaces and in TIR surface spectral properties (Figure 1). The least discolored, freshest looking sample (icel010, Figure 1e) is the only one that lacks obvious hydrated silicate features in the TIR spectrum of its natural surface. TIR spectroscopy laboratory work has demonstrated coatings as thin as $\sim$2 μm of hydrated silicates (silica or poorly crystalline aluminosilicates) can spectrally obscure the substrate [*Kraft et al.*, 2003; *Michalski et al.*, 2006], a situation that seems to apply here for the Icelandic samples. Only one displays nearly identical (montmorillonite) features on both natural and cut surfaces (hvalfj017), a result possibly explained by its XRD-determined bulk mineralogy of nearly 80% smectite.

5.4. Quantification With VNIR and TIR Spectroscopy

[52] As little as $\sim$10% smectite is observable in VNIR spectra of particulates of altered mafic rock samples, although phases do not always contribute to sample VNIR spectral properties in proportion to their abundance, complicating spectroscopic determinations of modal mineralogy. Given the XRD-determined abundances of smectite, the 2.3 μm absorption band depths of bulk-rock samples are smaller than expected, compared with band depths from man-made particulate mixtures of basalt and nontronite pure separates [*Ehlmann et al.*, 2010]. This is particularly evident in whole-rock samples (Figure 2 versus Figure 8) where metal-OH combination bands in some samples are nearly undetectable, possibly indicating that textural or surface properties affect band strength. Initial VNIR radiative transfer modeling of these samples using optical constants of nontronite, feldspars, pyroxenes, and glasses did not provide satisfactory modal mineralogy estimations [*Ehlmann et al.*, 2010]. Further study and nonlinear modeling will be needed to understand the conditions that limit mineral detection and quantitative abundance determination with VNIR spectroscopy.

[53] Modeling at TIR wavelengths using linear unmixing has been demonstrated to accuracies of 10–15% for crystalline igneous rocks [*Feely and Christensen*, 1999] but has not been rigorously investigated for altered rocks. Thin coatings appear to introduce nonlinear contributions to TIR spectra [*Kraft et al.*, 2003], so the use of linear unmixing on TIR spectra of altered rocks may be problematic. Given the apparent coatings on the Icelandic samples, modeling of bulk mineralogy probably is most valid using the spectra from cut surfaces or the one case where a coating is not readily apparent (icel010). In the NNLS modeling of all of the TIR emissivity spectra, smectites were correctly identified in all cases; however, there were considerable discrepancies between the quantity and composition of mineral phases modeled with TIR NNLS versus XRD (Tables 1 and 3). Nontronite is modeled as the dominant smectite in all samples (Figure 10), even though there is considerable compositional diversity in the actual smectite composition, probably including trioctahedral phases like ferrosaponites (Figure 7c). Trends in modeled abundances of pyroxene and plagioclase correlate with trends in actual abundances but pyroxene and feldspar content is universally underestimated and hydrated silicate content overestimated for all samples (Tables 1 and 3). Pyroxene and feldspar were not NNLS-modeled at all for the more altered rock samples though XRD shows they are the most abundant phases in the rock. Modeled NNLS results are typically more complex than XRD-derived results, including olivine (not present) and several, diverse hydrated silicates (more than XRD-identified). Restriction of the NNLS modeling to incorporate only XRD-identified phases resulted in higher RMS error values and qualitative fits did not improve (not shown).

[54] The overestimation of hydrated silicate phases in modeling results may be due in part to the fact that reference library samples of silicates did not provide good matches in composition and crystallinity to the actual phases present. Deformation bands in the 600–400 cm^{-1} range are rarely fit well in spite of the number of phases utilized (Figure 10). For example, in icel009 and icel010, the modeling of the stilbite, opal, and chlorite phases serves to subdue the contrast of nontronite's doublet feature so as to better fit the minima and shapes observed in the deformation band region. This overmodeling of hydrated silicates triggers a misfit (too narrow) in the Si-O stretch near 1000 cm^{-1}, which is then broadened by adding olivine. At present, few smectites are present in available TIR emission libraries, and feldspars are mostly well-ordered examples. Expansion of the mineral library to include more diverse compositionally variable phyllosilicate and zeolite mineral phases as well as disordered plagioclases, should improve the accuracy of NNLS unmixing results for altered, clay-bearing rocks. However, the inaccurate results obtained for these samples may be more a function of the nonlinear effects of coatings obscuring the substrate on natural surfaces and/or preferential alteration of grains where they are exposed on cut surfaces. This effect may be important on Mars, where thin surface coatings may mask underlying mineralogy. Different coating compositions might be expected because of different atmospheric compositions.

[55] The combined data sets acquired from the Icelandic samples provide some insights for interpreting spectral data from Mars. Among all of the samples, only one showed pervasive smectite alteration (hvlafj017), which was readily identified using both VNIR and TIR spectroscopy. Translated to locations on Mars where VNIR spectra identify smectites but TIR spectra do not, we can probably conclude

Table A1. Emission Spectra From the ASU Spectral Library Used for Unmixing

Class	Mineral	Sample ID
Feldspars	Albite	454, WAR-0612
	Andesine	434, BUR-240
	Andesine	561, WAS-0024
	Anorthite	564, BUR-340
	Anorthoclase	485, WAR-0579
	Bytownite	563, WAR-1384
	Labradorite	486, WAR-4524
	Labradorite	562, BUR-3080A
	Microcline	468, BUR-3460
	Oligoclase	450, WAR-0234
	Oligoclase	476, BUR-060
Pyroxenes	Augite	480, HS-119.4B
	Augite	494, BUR-620
	Augite	540, NMNH-119197
	Augite	554, DSM-AUG01
	Bronzite	439, BUR-1920
	Bronzite	541, NMNH-166555
	Bronzite	542, NMNH-119793
	Bronzite	552, NMNH-120414-1
	Bronzite	558, NMNH-93527
	Diopside	478, WAR-6474
	Diopside	547, NMNH-R15161
	Enstatite	458, HS-9.4B
	Hypersthene	442, NMNH-B18247
Olivines	Fayalite	557, WAR-FAY01
	Forsterite	441, BUR-3720A
	Olivine Fo18	959, KI 3354
	Olivine Fo39	956, KI 4143
	Olivine Fo54	955, KI 3372
	Olivine Fo68	953, KI 3115
Glasses	Andesite interstitial glass	1046, MEM-5
	Dacite interstitial glass	045, MEM-4
	K-rich glass	1736, K-rich glass
Oxides	Hematite	474, BUR-2600
	Ilmenite	463, WAR-4119
Phyllosilicates	Chlorite	466, WAR-1924
	Illite	596, IMt-2
	Kaolinite	571, KGa-1b
	Montmorillonite	583, SCa-3
	Montmorillonite (Ca)	582, STx-1
	Montmorillonite (Na)	585, SWy-2
	Nontronite	588, WAR-5108
	Saponite	579, Saponite
	Smectite	592, SWa-1
Silica-rich	Cristobalite	1968, Cristobalite
	Opal-A	1966, Opal-A
	Opal-CT	1972, Opal-CT
	Quartz	1969, Quartz
Zeolite	Heulandite	1840, agu_heu1
	Stilbite	1841, agu_stil

that such locations have not experienced pervasive alteration. Instead, they may represent more modest levels of alteration akin to all of the other samples in this study whose bulk smectite abundance is <25%. At these levels, VNIR spectra readily identify smectite phases that are more difficult to confirm with TIR spectra. We can further suggest from our results that Martian smectite occurrences likely do not represent thin coatings on rocks, given the ease with which they can be recognized with TIR spectra. To date, no unambiguous identification of smectite clays has been made on Mars using TIR spectra; relatively low abundance of such phases is one possible explanation and texture and temperature effects can also influence spectral contrast and phase detectability (for further discussion, see *Michalski and Fergason* [2009]).

5.5. Spectroscopy and XRD Synergies for Clay Mineral Identification

[56] MSL rover XRD measurements from CheMin used in conjunction with pattern libraries should permit excellent in situ quantitative characterization of modal mineralogy for powdered samples. Though considerable uncertainties remain in the estimation of abundance with VNIR and TIR spectroscopic data of altered samples, some important advantages exist in utilizing these spectral techniques, even beyond their ability to measure composition remotely rather than ingesting samples. They provide definitive information specifically related to the nature of the smectite component. VNIR spectroscopy is sensitive to shifts in absorption band position, providing information on the octahedral cations even when smectites are at small abundances in bulk samples. TIR spectroscopy is sensitive to thin phyllosilicate coatings and readily distinguishes dioctahedral from trioctahedral clays where present as the dominant phase. Only in the case of hvalf017 could the XRD 060 peak be resolved to determine that the smectite was dioctahedral. In other samples, interference from diffraction peaks from other minerals prevented determination of the nature of the smectite using XRD. On Mars, the CheMin instrument does not measure to sufficiently high 2θ angles (72°–74° required for Co radiation) to be able to measure this diagnostic feature nor can preparations with ethylene glycol be used to identified interstratified phases. Hence, a complimentary spectroscopic capability is best for determination of the octahedral cations (Fe/Mg versus Al) in smectite clays, even when in situ XRD mineralogic measurements are possible.

[57] The present generation of XRD technology measures ground, powdered samples, i.e., analyses are destructive. Our simple analysis of isolates from vesicle/fracture fills demonstrates that the ability to examine VNIR or TIR spectra from different portions of a rock at small scales (preferably nondestructively, unlike this study) permits identification of a greater number of minerals relative to what is possible from whole-rock spectra alone. This highlights the potential value of in situ instruments for small-scale spectroscopy that would permit mineralogic identifications at spatial scales of hundreds of micrometers [e.g., *Grady*, 2006; *Bibring and the Micromega Team*, 2008]. Although this capability does not replace the capabilities of laboratory analyses, e.g., electron microprobe, it provides a means of rapid, non-destructive analysis of the small-scale textural relationships between mineral phases that may elucidate the style of alteration and changes in fluid composition with time. Preservation of petrographic texture is key in discriminating clay formation environment on Earth and Mars [*Michalski et al.*, 2010a].

6. Conclusions

[58] VNIR spectra from hydrothermally altered and weathered lava flows in Iceland possess spectral signatures similar to those measured from Mars orbit. XRD analyses show that the bulk material in the Icelandic samples is smectite-bearing, and as little as 10% smectite is recognizable in VNIR spectra of these altered mafic rocks. Other alteration minerals such as zeolites, celadonite, and silica phases are concentrated primarily in vugs or fractures. Bulk-rock chemical data show scant evidence for chemical fractionation, but TIR and VNIR spectroscopy and XRD measurements identified distinctive assemblages of hydrous silicate minerals formed in distinctive

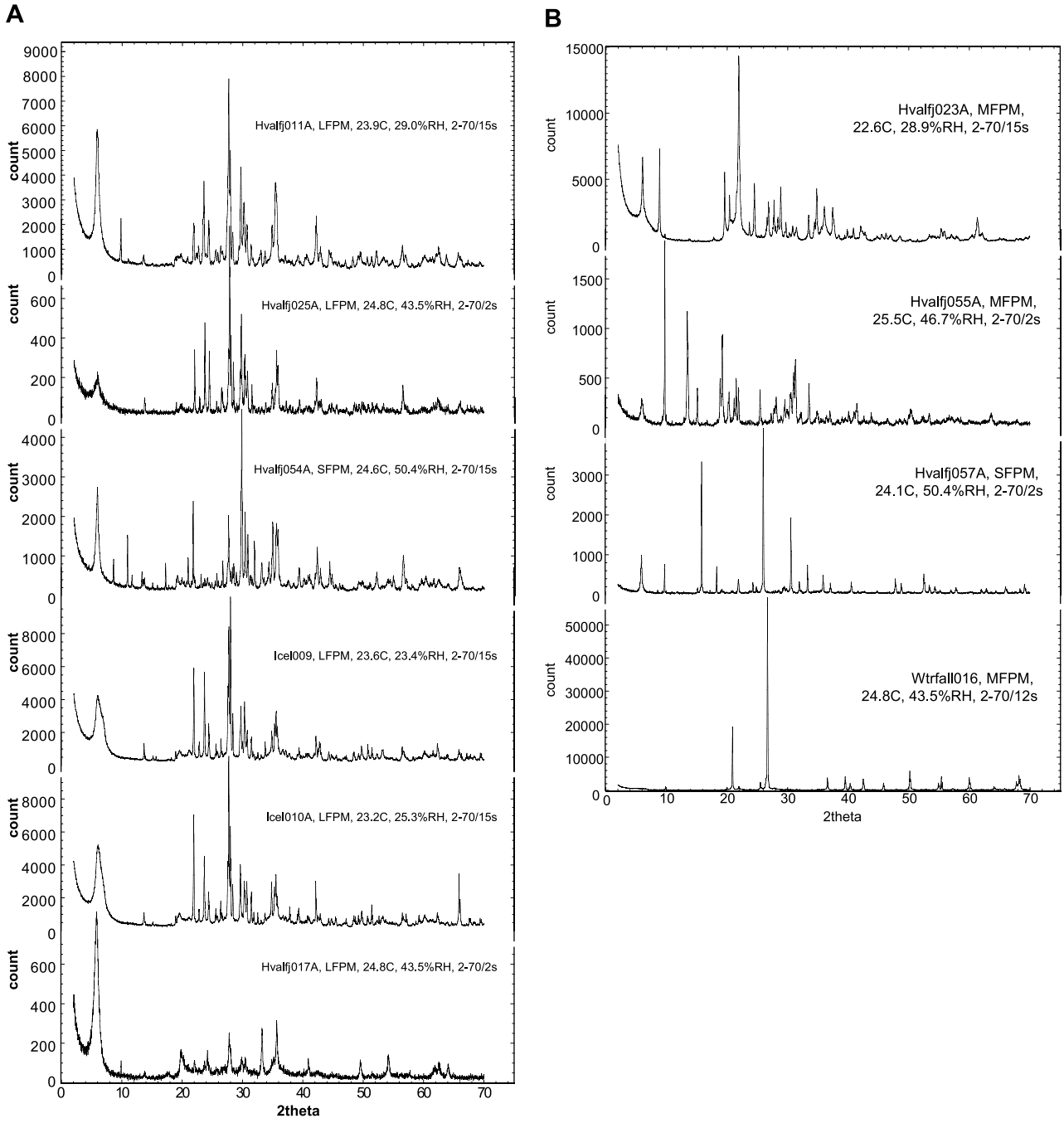

Figure A1. XRD patterns of bulk-rock and vesicle/fracture fill powdered samples from Icelandic rocks. The smectite 00ℓ peak near 2theta = 6 degrees is occasionally asymmetric, as in icel009 and icel010, because variable smectite hydration under ambient conditions results in variable interlayer spacing. Analyses with the NewMod program indicate <10% interstratified phase (section 4.1.1)

alteration environments. High spatial resolution mineralogical and chemical data sets were useful for understanding the texture and distribution of alteration products and variations in chemistry of altering fluids. Non-destructive means of making these measurements in petrographic context should be incorporated on future landed missions. XRD was found to provide the most complete and accurate quantitative determination of sample modal mineralogy; however, VNIR spectroscopy was the in situ technique most useful for identification of the composition of smectite clays at low abundance and TIR spectroscopy was the most useful for recognizing hydrated silicates in thin surface coatings.

[59] The full sample mineralogy is not completely captured by VNIR spectroscopic data because of masking of some minerals' signatures by others. TIR spectroscopic data are sensitive to alteration but in this case provide inaccurate

Table A2. Results of Flux Fusion Elemental Analysis for Iceland Samples (wt. %)

Sample	Al_2O_3	CaO	Fe_2O_3(T)	K_2O	MgO	MnO	Na_2O	SiO_2	TiO_2	Total
hvalfj011C	14.54 ± 0.54	9.95 ± 0.51	10.78 ± 0.47	1.30 ± 0.026	7.10 ± 0.22	0.17 ± 0.005	1.67 ± 0.14	48.21 ± 2.19	2.05 ± 0.08	95.78 ± 4.11
hvalfj017C	15.28 ± 0.42	5.48 ± 0.053	15.14 ± 0.42	0.73 ± 0.04	3.84 ± 0.13	0.17 ± 0.005	1.46 ± 0.15	44.05 ± 0.91	3.72 ± 0.16	89.92 ± 1.84
hvalfj023C	3.99 ± 0.065	1.15 ± 0.094	16.88 ± 0.70	3.40 ± 0.06	2.76 ± 0.054	0.21 ± 0.005	0.62 ± 0.13	62.21 ± 2.84	0.54 ± 0.03	91.58 ± 3.40
hvalfj025C	11.70 ± 0.32	8.75 ± 0.18	20.73 ± 0.86	0.40 ± 0.02	4.704 ± 0.18	0.026 ± 0.001	2.42 ± 0.21	42.74 ± 1.04	6.51 ± 0.34	98.23 ± 2.90
hvalfj054C	9.84 ± 0.20	12.59 ± 0.65	15.45 ± 0.44	0.053 ± 0.005	9.05 ± 0.083	0.27 ± 0.007	1.09 ± 0.12	42.87 ± 1.58	3.34 ± 0.11	94.56 ± 2.95
hvalfj055C	27.08 ± 0.62	11.64 ± 0.61	1.16 ± 0.066	0.004 ± 0.001	0.77 ± 0.027	0.26 ± 0.007	4.00 ± 0.12	45.50 ± 1.36	0.13 ± 0.005	90.30 ± 2.59
hvalfj057C	22.03 ± 0.67	1.11 ± 0.098	1.10 ± 0.04	0.010 ± 0.009	0.83 ± 0.02	0.024 ± 0.002	10.89 ± 0.05	54.50 ± 2.70	0.018 ± 0.002	90.52 ± 3.28
icel009C	11.20 ± 1.58	6.89 ± 0.99	17.03 ± 2.60	0.93 ± 0.12	4.20 ± 0.57	0.019 ± 0.001	2.58 ± 0.19	43.75 ± 6.53	3.56 ± 0.54	90.35 ± 13.16
icel010C	10.75 ± 1.60	7.02 ± 1.14	16.55 ± 2.98	0.84 ± 0.13	4.31 ± 0.70	0.20 ± 0.035	2.52 ± 0.22	43.01 ± 7.15	4.40 ± 0.65	89.61 ± 14.60
wtrfall016C	0.36 ± 0.026	(−0.02 ± 0.001)	0.17 ± 0.016	0.022 ± 0.003	0.042 ± 0.0003	0.002 ± 0.0001	0.29 ± 0.007	96.96 ± 2.56	0.027 ± 0.015	97.85 ± 2.53

quantitative compositional estimates because of nonlinear mixing effects and differences between library and sample silicate composition and crystallinity. Nevertheless, spectral data capture the principal mineralogic diversity, and provide a means of rapidly assessing the extent and nature of past alteration. Examination of rocks from Mars orbit, even at large scales, similarly should provide effective information on the mineral assemblages present on the surface. XRD quantitative mineralogy along with geochemistry of samples measured here may be similar to what a rover mission would measure with in situ instruments at some of Mars' largest clay-bearing terrains. This study highlights the importance of ground-truthing spectral data from Mars and improving techniques for quantitative remote determination of modal mineralogy. This study also demonstrates how spectroscopy can provide most of the information about key mineral assemblages and, especially for low abundance smectite-bearing materials, provide important supplemental compositional information for interpreting in situ XRD and geochemical analysis. Use of a combination of measurements to characterize the mineralogy of alteration on Mars lends confidence to inferences of past environmental processes. Understanding the linkages between remote spectroscopic and in situ data will be critical to successful traverse planning, data interpretation, and understanding past environmental conditions on Mars.

Appendix A

[60] Library thermal emission spectra used in non-negative least squares unmixing of thermal emission data from the Icelandic samples (see section 3.4 and 4.4.2) are listed in Table A1. XRD patterns used in relative-intensity-ratio and Rietveld refinement determinations of modal mineralogy (see section 4.1) are provided in Figure A1. Bulk rock major element compositions for the samples discussed in section 4.2 are tabulated in Table A2.

[61] **Acknowledgments.** This work benefited from the invaluable advice and laboratory assistance provided by Dave Murray (flux fusion analysis), Joe Orchardo (ICP-OES), Bill Collins (thin section preparation), Joe Devine (microprobe), Taki Hiroi (RELAB spectral measurements), Miles Watkins (rock sample cataloging), and Michael Cheshire (XRD measurement assistance). Thanks to Mike Wyatt, Ulyana Horodyskyj, and Richard Lewis for supporting field work and comments by Christina Viviano and an anonymous reviewer, which improved this work.

References

Anderson, J. H., and K. A. Wickersheim (1964), Near infrared characterization of water and hydroxyl groups on silica surfaces, *Surf. Sci.*, *2*, 252–260, doi:10.1016/0039-6028(64)90064-0.

Arnórsson, S. (1995a), Geothermal systems in Iceland: Structure and conceptual models—II. Low-temperature areas, *Geothermics*, *24*(5–6), 561–602, doi:10.1016/0375-6505(95)00025-9.

Arnórsson, S. (1995b), Geothermal systems in Iceland: Structure and conceptual models—II. Low-temperature areas, *Geothermics*, *24*(5–6), 603–629, doi:10.1016/0375-6505(95)00026-7.

Bandfield, J. L., V. E. Hamilton, P. R. Christensen, and H. Y. McSween Jr. (2004), Identification of quartzofeldspathic materials on Mars, *J. Geophys. Res.*, *109*, E10009, doi:10.1029/2004JE002290.

Benison, K. C., B. B. Bowen, F. E. Oboh-Ikuenobe, E. A. Jagniecki, D. A. LaClair, S. L. Story, M. R. Mormile, and B.-Y. Hong (2007), Sedimentology of acid lakes in southern Western Australia: Newly described processes and products of an extreme environment, *J. Sediment. Res.*, *77*, 366–388, doi:10.2110/jsr.2007.038.

Bibring, J.-P., and the Micromega Team (2008), The MicrOmega/ExoMars investigation, Abstract 1441 presented at Workshop on Martian Phyllosilicates: Recorders of Aqueous Processes?, Lunar and Planet. Inst., Paris, 21–23 October.

Bibring, J.-P., et al. (2005), Mars surface diversity as revealed by the OMEGA/Mars Express Observations, *Science*, *307*, 1576–1581, doi:10.1126/science.1108806.

Bibring, J.-P., et al. (2006), Global mineralogical and aqueous Mars history derived from OMEGA/Mars Express data, *Science*, *312*, 400–404, doi:10.1126/science.1122659.

Bish, D. L., and S. J. Chipera (1991), Detection of trace amounts of erionite using X-ray powder diffraction: Erionite in tuffs of Yucca Mountain, Nevada, and central Turkey, *Clays Clay Miner.*, *39*, 437–445, doi:10.1346/CCMN.1991.0390413.

Bish, D. L., and J. E. Post (1993), Quantitative mineralogical analysis using the Rietveld full-pattern fitting method, *Am. Mineral.*, *78*, 932–940.

Bishop, J. L., C. M. Pieters, and J. O. Edwards (1994), Infrared spectroscopic analyses on the nature of water in montmorillonite, *Clays Clay Miner.*, *42*(6), 702–716, doi:10.1346/CCMN.1994.0420606.

Bishop, J. L., P. Schiffman, and R. Southard (2002a), Geochemical and mineralogical analyses of palagonitic tuffs and altered rinds of pillow basalts in Iceland and applications to Mars, in *Volcano-Ice Interaction on Earth and Mars*, edited by J. L. Smellie and M. G. Chapman, *Geol. Soc. Spec. Publ.*, *202*, 371–392.

Bishop, J., J. Madejova, P. Komadel, and H. Froschl (2002b), The influence of structural Fe, Al, and Mg on the infrared OH bands in spectra of dioctahedral smectites, *Clay Miner.*, *37*, 607–616, doi:10.1180/0009855023740063.

Bishop, J. L., E. Murad, and M. D. Dyar (2002c), The influence of octahedral and tetrahedral cation substitution on the structure of smectites and serpentines as observed through infrared spectroscopy, *Clay Miner.*, *37*, 617–628, doi:10.1180/0009855023740064.

Bishop, J. L., et al. (2008a), Phyllosilicate diversity and past aqueous activity revealed at Mawrth Vallis, Mars, *Science*, *321*, 830–833, doi:10.1126/science.1159699.

Bishop, J. L., M. D. Lane, M. D. Dyar, and A. J. Brown (2008b), Reflectance and emission spectroscopy of four groups of phyllosilicates: Smectites, kaolinite-serpentines, chlorites, and micas, *Clay Miner.*, *43*, 35–54, doi:10.1180/claymin.2008.043.1.03.

Blake, D. F., et al. (2010), Test and delivery of the CheMin mineralogical instrument for the Mars Science Laboratory, *Lunar Planet. Sci.*, *XLI*, Abstract 1898.

Burns, R. G. (1993), *Mineralogical Applications of Crystal-Field Theory*, 551 pp., Cambridge Univ. Press, Cambridge, U. K., doi:10.1017/CBO9780511524899.

Carter, J., F. Poulet, J. P. Bibring, and S. Murchie (2010), Detection of hydrated silicates in crustal outcrops in the northern plains of Mars, *Science*, *328*, 1682–1686, doi:10.1126/science.1189013.

Chipera, S. J., G. D. Guthrie, and D. L. Bish (1993), Preparation and purification of mineral dusts, in *Health Effects of Mineral Dust*, *Rev Mineral.*, vol. 28, edited by G. D. Guthrie and B. T. Mossman, pp. 235–249, Mineral. Soc. of Am., Washington, D. C.

Christensen, P. R., J. L. Bandfield, V. E. Hamilton, D. A. Howard, M. D. Lane, J. L. Piatek, S. W. Ruff, and W. L. Stefanov (2000), A thermal emission spectral library of rock forming minerals, *J. Geophys. Res.*, *105*(E4), 9735–9739, doi:10.1029/1998JE000624.

Christensen, P. R., et al. (2001), Mars Global Surveyor Thermal Emission Spectrometer experiment: Investigation description and surface science results, *J. Geophys. Res.*, *106*(E10), 23,823–23,871, doi:10.1029/2000JE001370.

Christensen, P. R., et al. (2003), Miniature Thermal Emission Spectrometer for the Mars Exploration Rovers, *J. Geophys. Res.*, *108*(E12), 8064, doi:10.1029/2003JE002117.

Chung, F. H. (1974), Quantitative interpretation of X-ray diffraction patterns of mixtures. II. Adiabatic principle of X-ray diffraction analysis of mixtures, *J. Appl. Crystallogr.*, *7*, 526–531, doi:10.1107/S0021889874010387.

Clark, R. N., T. V. V. King, M. Klejwa, G. A. Swayze, and N. Vergo (1990), High resolution reflectance spectroscopy of minerals, *J. Geophys. Res.*, *95*(B8), 12,653–12,680, doi:10.1029/JB095iB08p12653.

Clark, R. N., G. A. Swayze, R. Wise, K. E. Livo, T. M. Hoefen, R. F. Kokaly, and S. J. Sutley, (2007), USGS Digital Spectral Library splib06a, *U.S. Geol. Surv. Data Ser.*, *231*.

Cloutis, E. A., P. M. Asher, and S. A. Mertzman (2002), Spectral reflectance properties of zeolites and remote sensing implications, *J. Geophys. Res.*, *107*(E9), 5067, doi:10.1029/2000JE001467.

Ehlmann, B. L., et al. (2009), Identification of hydrated silicate minerals on Mars using MRO-CRISM: Geologic context near Nili Fossae and implications for aqueous alteration, *J. Geophys. Res.*, *114*, E00D08, doi:10.1029/2009JE003339.

Ehlmann, B. L., J. F. Mustard, D. L. Bish, and F. Poulet (2010), How much clay is on Mars? Lessons from visible/near-infrared (VNIR) and XRD study of hydrated silicate mineral assemblages in altered basalts from Iceland, Abstract IMS3-PS-9 presented at the First Moscow Solar System Symposium, Space Res. Inst. of the Russ. Acad. of Sci., Moscow, 11–15 October.

Ehlmann, B. L., et al. (2011a), Subsurface water and clay mineral formation during the early history of Mars, *Nature*, *479*, 53–60, doi:10.1038/nature10582.

Ehlmann, B. L., J. F. Mustard, R. N. Clark, G. A. Swayze, and S. L. Murchie (2011b), Evidence for low-grade metamorphism, diagenesis, and hydrothermal alteration on Mars from phyllosilicate mineral assemblages, *Clays Clay Miner.*, *59*, 359–377, doi:10.1346/CCMN.2011.0590402.

Farmer, V. C. (1974), *The Infrared Spectra of Minerals*, *Mineral. Soc. Monogr.*, *4*, 539 pp.

Feely, K. C., and P. R. Christensen (1999), Quantitative compositional analysis using thermal emission spectroscopy: Application to igneous and metamorphic rocks, *J. Geophys. Res.*, *104*(E10), 24,195–24,210, doi:10.1029/1999JE001034.

Fernández-Remolar, D. C., et al. (2005), The Rio Tinto Bain, Spain: Mineralogy, sedimentary geobiology, and implications for interpretation of outcrop rocks at Meridiani Planum, Mars, *Earth Planet. Sci. Lett.*, *240*, 149–167, doi:10.1016/j.epsl.2005.09.043.

Franzson, J., R. Zierenberg, and P. Schiffman (2008), Chemical transport in geothermal systems in Iceland: Evidence from hydrothermal alteration, *J. Volcanol. Geotherm. Res.*, *173*, 217–229, doi:10.1016/j.jvolgeores.2008.01.027.

Frost, R. L., J. T. Kloprogge, and Z. Ding (2002), Near-infrared spectroscopic study of nontronites and ferruginous smectite, *Spectrochim. Acta Part A*, *58*, 1657–1668.

Gates, W. P. (2005), Infrared spectroscopy and the chemistry of dioctahedral smectites, in *Vibrational Spectroscopy of Layer Silicates and Hydroxides*, *CMS Workshop Lectures*, vol. 13, edited by T. Kloprogge, pp. 125–168, Clay Minerals Soc., Aurora, Colo.

Gislason, S. R., and H. P. Eugster (1987), Meteoric water-basalt interactions: II. A field study in NE Iceland, *Geochim. Cosmochim. Acta*, *51*, 2841–2855, doi:10.1016/0016-7037(87)90162-1.

Gislason, S. R., S. Arnórsson, and H. Armannsson (1996), Chemical weathering of basalt in southwest Iceland: Effects of runoff, age of rocks, and vegetative/glacial cover, *Am. J. Sci.*, *296*, 837–907, doi:10.2475/ajs.296.8.837.

Goryniuk, M. C., B. A. Rivard, and B. Jones (2004), The reflectance spectra of opal-A, 0.5–25 um) from the Taupo Volcanic zone: Spectra that may identify hydrothermal systems on planetary surfaces, *Geophys. Res. Lett.*, *31*, L24701, doi:10.1029/2004GL021481.

Grady, M. M. (2006), WatSen: Searching for clues for water (and life) on Mars, *Int. J. Astrobiol.*, *5*(3), 211–219, doi:10.1017/S1473550406003077.

Grauby, O., S. Petit, A. Decarreau, and A. Baronnet (1994), The nontronite-saponite series: An experimental approach, *Eur. J. Mineral.*, *6*, 99–112.

Grotzinger, J. P., et al. (2012), Mars Science Laboratory mission and science investigation, *Space Sci. Rev.*, *170*, 5–56, doi:10.1007/s11214-012-9892-2.

Hamilton, V. E., R. V. Morris, J. E. Gruener, and S. A. Mertzman (2008), Visible, near infrared, and middle infrared spectroscopy of altered basaltic tephras: Spectral signatures of phyllosilicates, sulfates, and other aqueous alteration products with application to the mineralogy of the Columbia Hills of Gusev crater, Mars, *J. Geophys. Res.*, *113*, E12S43, doi:10.1029/2007JE003049.

Hunt, G. R., J. W. Salisbury, and C. J. Lenhoff, (1973), Visible and near infrared spectra of minerals and rocks: VI. Additional silicates. *Modern Geology*, *4*, 85–106.

Hurowitz, J. A., and S. M. McLennan (2007), A 3.5 Ga record of water-limited, acidic weathering conditions on Mars, *Earth Planet. Sci. Lett.*, *260*, 432–443, doi:10.1016/j.epsl.2007.05.043.

Kissel, C., et al. (2010), Emplacement of magma in Eastern Iceland dikes: Insights from magnetic fabric and rock magnetic analyses, *J. Volcanol. Geotherm. Res.*, *191*, 79–92, doi:10.1016/j.jvolgeores.2009.12.008.

Kraft, M. D., J. R. Michalski, and T. G. Sharp (2003), Effects of pure silica coatings on thermal emission spectra of basaltic rocks: Considerations for Martian surface mineralogy, *Geophys. Res. Lett.*, *30*(24), 2288, doi:10.1029/2003GL018848.

Kristmannsdottir, H. (1976), Types of clay minerals in hydrothermally altered basaltic rocks, Reykjanes, Iceland, *Jökull*, *26*, 30–39.

Li, G., D. R. Peacor, D. S. Coombs, and Y. Kawachi (1997), Solid solution in the celadonite family: The new minerals ferroceladonite, $K_2Fe_2^{2+}Fe_2^{3+}Si_8O_{20}(OH)_4$, and ferroaluminoceladonite, $K_2Fe_2^{2+}Al_2Si_8O_{20}(OH)_4$, *Am. Mineral.*, *82*, 503–511.

Loizeau, D., et al. (2010), Stratigraphy in the Mawrth Vallis region through OMEGA, HRSC color imagery, and DTM, *Icarus*, *205*, 396–418, doi:10.1016/j.icarus.2009.04.018.

Lonker, S. W., H. Franzson, and H. Kristmannsdottir (1993), Mineral-fluid interactions in the Reykjanes and Svartsengi geothermal systems, Iceland, *Am. J. Sci.*, *293*, 605–670, doi:10.2475/ajs.293.7.605.

Marks, N., et al. (2010), Hydrothermal alteration in the Reykjanes geothermal system: Insights from Iceland deep drilling program well RN-17,

J. Volcanol. Geotherm. Res., *189*, 172–190, doi:10.1016/j.jvolgeores.2009.10.018.

McDowell, M. L., and V. E. Hamilton (2009), Seeking phyllosilicates in thermal infrared data: A laboratory and Martian data case study, *J. Geophys. Res.*, *114*, E06007, doi:10.1029/2008JE003317.

Michalski, J. R., and R. L. Fergason (2009), Composition and thermal inertia of the Mawrth Vallis region of Mars from TES and THEMIS; data, *Icarus*, *199*, 25–48, doi:10.1016/j.icarus.2008.08.016.

Michalski, J. R., M. D. Kraft, T. Diedrich, T. G. Sharp, and P. R. Christensen (2003), Thermal emission spectroscopy of the silica polymorphs and considerations for remote sensing of Mars, *Geophys. Res. Lett.*, *30*(19), 2008, doi:10.1029/2003GL018354.

Michalski, J. R., M. D. Kraft, R. P. Sharp, L. B. Williams, and P. R. Christensen (2005), Mineralogical constraints on the high-silica Martian surface component observed by TES, *Icarus*, *174*, 161–177, doi:10.1016/j.icarus.2004.10.022.

Michalski, J. R., M. D. Kraft, T. G. Sharp, and P. R. Christensen (2006), Effects of chemical weathering on infrared spectra of Columbia River Basalt and spectral interpretation of Martian alteration, *Earth Planet. Sci. Lett.*, *248*(3–4), 822–829, doi:10.1016/j.epsl.2006.06.034.

Michalski, J. R., et al. (2010a), The Mawrth Vallis Region of Mars: A Potential Landing Site for the Mars Science Laboratory (MSL) Mission, *Astrobiology*, *10*(7), 687–703, doi:10.1089/ast.2010.0491.

Michalski, J. R., F. Poulet, J.-P. Bibring, and N. Mangold (2010b), Analysis of phyllosilicate deposits in the Nili Fossae region of Mars: Comparison of TES and OMEGA data, *Icarus*, *206*, 269–289, doi:10.1016/j.icarus.2009.09.006.

Milliken, R. E., et al. (2008), Opaline silica in young deposits on Mars, *Geology*, *36*(11), 847–850, doi:10.1130/G24967A.1.

Milliken, R. E., J. P. Grotzinger, and B. J. Thomson (2010), Paleoclimate of Mars as captured by the stratigraphic record in Gale Crater, *Geophys. Res. Lett.*, *37*, L04201, doi:10.1029/2009GL041870.

Moore, D., and R. C. Reynolds Jr. (1997), *X-Ray Diffraction and the Identification and Analysis of Clay Minerals*, 2nd ed., Oxford Univ. Press, New York.

Morris, R. V., et al. (2005), Hematite spherules in basaltic tephra altered under aqueous, acid-sulfate conditions on Mauna Kea volcano, Hawaii: Possible clues for the occurrence of hematite-rich spherules in the Burns formation at Meridiani Planum, Mars, *Earth Planet. Sci. Lett.*, *240*, 168–178, doi:10.1016/j.epsl.2005.09.044.

Morris, R. V., T. G. Graff, C. N. Achilles, D. G. Agresti, D. W. Ming, and D. C. Golden (2011), Visible and near-IR reflectance spectra of Mars analogue materials under aird conditions for interpretation of Martian surface mineralogy, *Lunar Planet. Sci.*, *XLII*, Abstract 2757.

Murchie, S. L., et al. (2007), Compact Reconnaissance Imaging Spectrometer for Mars, CRISM) on Mars Reconnaissance Orbiter, MRO, *J. Geophys. Res.*, *112*, E05S03, doi:10.1029/2006JE002682.

Murchie, S. L., et al. (2009), A synthesis of Martian aqueous mineralogy after one Mars year of observations from the Mars Reconnaissance Orbiter, *J. Geophys. Res.*, *114*, E00D06, doi:10.1029/2009JE003342.

Murray, R. W., D. J. Miller, and K. A. Kryc (2000), Analysis of major and trace elements in rocks, sediments, and interstitial waters by inductively coupled plasma–atomic emission spectrometry, ICP-AES), *ODP Tech. Note*, *29*, 27 pp., [Available at http://www-odp.tamu.edu/publications/tnotes/tn29/INDEX.HTM].

Mustard, J. F., and J. E. Hays (1997), Effects of hyperfine particles on reflectance spectra from 0.3–25 μm, *Icarus*, *125*, 145–163, doi:10.1006/icar.1996.5583.

Mustard, J. F., et al. (2008), Hydrated silicate minerals on Mars observed by the CRISM instrument on MRO, *Nature*, *454*, 305–309, doi:10.1038/nature07097.

Neuhoff, P. S., T. Fridriksson, S. Arnórsson, and D. K. Bird (1999), Porosity evolution and mineral paragenesis during low-grade metamorphism of basaltic lavas at Teigarhorn, eastern Iceland, *Am. J. Sci.*, *299*, 467–501, doi:10.2475/ajs.299.6.467.

Pieters, C. M. (1983), Strength of mineral absorption features in the transmitted component of near-infrared reflected light: First results from RELAB, *J. Geophys. Res.*, *88*(B11), 9534–9544, doi:10.1029/JB088iB11p09534.

Poulet, F., et al. (2005), Phyllosilicates on Mars and implications for early Martian climate, *Nature*, *438*, 623–627, doi:10.1038/nature04274.

Poulet, F., N. Mangold, D. Loizeau, J.-P. Bibring, Y. Langevin, J. Michalski, and B. Gondet (2008), Abundance of minerals in the phyllosilicate-rich units on Mars, *Astron. Astrophys.*, *487*, L41–L44, doi:10.1051/0004-6361:200810150.

Rogers, A. D., and O. Aharonson (2008), Mineralogical composition of sands in Meridiani Planum determined from Mars Exploration Rover data and comparison to orbital measurements, *J. Geophys. Res.*, *113*, E06S14, doi:10.1029/2007JE002995.

Ruff, S. W. (2004), Spectral evidence for zeolite in the dust on Mars, *Icarus*, *168*, 131–143, doi:10.1016/j.icarus.2003.11.003.

Ruff, S. W., and P. R. Christensen (2007), Basaltic andesite, altered basalt, and a TES-based search for smectite clay minerals on Mars, *Geophys. Res. Lett.*, *34*, L10204, doi:10.1029/2007GL029602.

Ruff, S. W., P. R. Christensen, P. W. Barbera, and D. L. Anderson (1997), Quantitative thermal emission spectroscopy of minerals: A laboratory technique for measurement and calibration, *J. Geophys. Res.*, *102*(B7), 14,899–14,913, doi:10.1029/97JB00593.

Salisbury, J. W., and J. W. Eastes (1985), The effect of particle size and porosity on spectral contrast in the mid-infrared, *Icarus*, *64*, 586–588, doi:10.1016/0019-1035(85)90078-8.

Salisbury, J. W., L. S. Walter, N. Vergo, and D. M. D'Aria (1991), *Infrared (2.1–25 μm) Spectra of Minerals*, 267 pp., Johns Hopkins Univ. Press, Baltimore, Md.

Schiffman, P., et al. (2006), Acid-fog deposition at Kilauea volcano: A possible mechanism for the formation of siliceous-sulfate rock coatings on Mars, *Geology*, *34*(11), 921–924.

Seelos, K. D., R. E. Arvidson, B. L. Jolliff, S. M. Chemtob, R. V. Morris, D. W. Ming, and G. A. Swayze (2010), Silica in a Mars analog environment: Ka'u Desert, Kilauea Volcano, Hawaii, *J. Geophys. Res.*, *115*, E00D15, doi:10.1029/2009JE003347.

Stolper, E. (1982), Water in silicate glasses: An infrared spectroscopic study, *Contrib. Mineral. Petrol.*, *81*, 1–17, doi:10.1007/BF00371154.

Swayze, G. A., et al. (2007), Spectral evidence for hydrated volcanic and/or impact glass on Mars with MRO CRISM, in *Seventh International Conference on Mars, July 9–13, 2007, Pasadena CA* [CD-ROM], *LPI Contrib.*, *1353*, Abstract 3384.

Taylor, G. J., L. M. V. Martel, S. Karunatillake, O. Gasnault, and W. V. Boynton (2010), Mapping Mars geochemically, *Geology*, *38*(2), 183–186, doi:10.1130/G30470.1.

Walter, L. S., and J. W. Salisbury (1989), Spectral characterization of igneous rocks in the 8− to 12− um region, *J. Geophys. Res.*, *94*(B7), 9203–9213, doi:10.1029/JB094iB07p09203.

Weisenberger, T., and R. S. Selbekk (2009), Multi-stage zeolite facies mineralization in the Hvalfjordur area, Iceland, *Int. J. Earth Sci.*, *98*(5), 985–999, doi:10.1007/s00531-007-0296-6.

Wray, J. J., B. L. Ehlmann, S. W. Squyres, J. F. Mustard, and R. L. Kirk (2008), Compositional stratigraphy of clay-bearing layered deposits at Mawrth Vallis, Mars, *Geophys. Res. Lett.*, *35*, L12202, doi:10.1029/2008GL034385.

Wyatt, M. B., and H. Y. McSween Jr. (2002), Spectral evidence for weathered basalt as an alternative to andesite in the northern lowlands of Mars, *Nature*, *417*, 263–266, doi:10.1038/417263a.

Wyatt, M. B., et al. (2001), Analysis of terrestrial and Martian volcanic compositions using thermal emission spectroscopy: I. Determination of mineralogy, chemistry, and classification strategies, *J. Geophys. Res.*, *106*(E7), 14,711–14,732, doi:10.1029/2000JE001356.

Yuan, H., and D. L. Bish (2010), NEWMOD+, a new version of the NEWMOD program for interpreting x-ray powder diffraction patterns from interstratified clay minerals. *Clays and Clay Minerals*, *58*(3), 318–326, doi: 10.1346/CCMN.2010.0580303.